Mon. Not. R. Astron. Soc. **000**, 1–20 (2013) Printed 14 January 2014 (MN LATEX style file v2.2)

Physics input for modelling superfluid neutron stars with hyperon cores

M. E. Gusakov[1,2⋆], P. Haensel[3]†, E. M. Kantor[1]‡,
[1] *Ioffe Physical-Technical Institute of the Russian Academy of Sciences, Polytekhnicheskaya 26, 194021 Saint-Petersburg, Russia*
[2] *Saint-Petersburg State Polytechnical University, Polytekhnicheskaya 29, 195251 St.-Petersburg, Russia*
[3] *N. Copernicus Astronomical Center, Polish Academy of Sciences, Bartycka 18, PL-00-716 Warszawa, Poland*

Accepted 2013 xxxx. Received 2013 xxxx; in original form 2013 xxxx

arXiv:1401.2827v1 [astro-ph.HE] 13 Jan 2014

ABSTRACT

Observations of massive ($M \approx 2.0$ M$_\odot$) neutron stars (NSs), PSRs J1614-2230 and J0348+0432, rule out most of the models of nucleon-hyperon matter employed in NS simulations. Here we construct three possible models of nucleon-hyperon matter consistent with the existence of 2 M$_\odot$ pulsars as well as with semi-empirical nuclear matter parameters at saturation, and semi-empirical hypernuclear data. Our aim is to calculate for these models all the parameters necessary for modelling dynamics of hyperon stars (such as equation of state, adiabatic indices, thermodynamic derivatives, relativistic entrainment matrix, etc.), making them available for a potential user. To this aim a general non-linear hadronic Lagrangian involving $\sigma\omega\rho\phi\sigma^*$ meson fields, as well as quartic terms in vector-meson fields, is considered. A universal scheme for calculation of the $\ell = 0, 1$ Landau Fermi-liquid parameters and relativistic entrainment matrix is formulated in the mean-field approximation. Use of this scheme allow us to obtain numerical tables with the equation of state, Landau quasiparticle effective masses, adiabatic indices, the $\ell = 0, 1$ Landau Fermi-liquid parameters, and the relativistic entrainment matrix for the selected models of nucleon-hyperon matter. These data are available on-line and suitable for numerical implementation in computer codes modelling various dynamical processes in NSs, in particular, oscillations of superfluid NSs and their cooling.

Key words: stars: interiors - stars: neutron - stars: oscillations

1 INTRODUCTION

Neutron stars (NSs), being massive, compact, rapidly rotating objects, with central density up to ten times normal nuclear density ($\rho_0 \approx 2.8 \times 10^{14}$ g cm^{-3}, corresponding to baryon number density $n_0 \approx 0.16$ fm^{-3}), are promising sources of gravitational waves, associated with axial-symmetry breaking stellar pulsations, triggered by various types of instabilities (Andersson et al. 2011, 2013). Modelling NS dynamics requires hydrodynamical description of its liquid core, of density ranging from $\sim 0.5\rho_0$ at the outer edge of the core, to $\sim 10\rho_0$ at the centre of the most massive stars. It is expected that the core layer up to $2 - 3\rho_0$, called the outer core, consists of nucleons (mostly neutrons) and leptons (electrons and muons), while at higher density (inner core) the matter is expected to contain also hyperons. We are then dealing with a baryon matter, consisting of more than two baryon species (to be contrasted with nuclear matter in the outer core), with an admixture of leptons required by weak-interaction equilibrium and charge neutrality. At least some of the baryon species are thought to be superfluid.

To study dynamics of a multi-superfluid nucleon-hyperon (NH) matter, one needs not only the equation of state (EOS), involving various thermodynamic derivatives, but also a (symmetric) relativistic entrainment matrix Y_{ij} (hereafter subscripts i, j run over all baryon species), describing non-dissipative interaction between superfluids due to strong interaction of baryons.

⋆ gusakov@astro.ioffe.ru
† haensel@camk.edu.pl
‡ kantor@mail.ioffe.ru

A method of the calculation of Y_{ij} for a mixture of NH superfluids was presented in the limiting case of zero temperature ($T = 0$) in Gusakov, Kantor & Haensel (2009b) and then generalized to non-zero T in Gusakov, Kantor & Haensel (2009a). Strong interactions between baryons were included using relativistic extension (Baym & Chin 1976) of the Landau theory of Fermi liquids.

Numerical results of Gusakov et al. (2009b,a) were obtained employing a basic version of the relativistic mean field model (RMF; see Glendenning 2000, 1985 and references therein). This RMF model involved the baryon octet, interacting via coupling to scalar (σ), vector (ω^μ), and vector-isovector (ρ^μ_a) meson fields; here μ and a indices denote the spacetime and isospin components of the field, respectively. Unfortunately, the model used in Gusakov et al. (2009b,a) is not consistent with up-to-date hypernuclear data.

In the present paper we replace the $\sigma\omega\rho$ Lagrangian by a more general non-linear model involving two additional hidden-strangeness mesons (Bednarek & Manka 2009 and references therein). In this way we are able to overcome the shortcomings of Gusakov et al. (2009b,a). Our models fulfil constraint on the maximum NS mass $M_{\rm max} > 2$ M$_\odot$ resulting from the discovery of 2 M$_\odot$ pulsars (Demorest et al. 2010; Antoniadis et al. 2013). They are consistent with semi-empirical saturation parameters of nuclear matters, binding energies of Λ and Ξ^- hyperons in nuclear matter deduced from hypernuclei, and reproduce potential well for Σ^- in nuclear matter deduced from the Σ^- atoms. As shown in several recent papers (Bednarek et al. 2012; Weissenborn, Chatterjee & Schaffner-Bielich 2012a,b), all these constraints can be simultaneously satisfied by introducing an additional vector meson field ϕ coupled only to hyperons, resulting in a strong hyperon repulsion at high densities, and/or allowing for breaking of SU(6) symmetry in the vector-mesons coupling to hyperons. Therefore, instead of a (too) simple $\sigma\omega\rho$ model, used in Gusakov et al. (2009b,a), we consider at least the $\sigma\omega\rho\phi$ one. In order to get a better fit to a larger number of semi-empirical hyper-nuclear parameters (e.g., to describe a weak $\Lambda - \Lambda$ interaction following from 'Nagara' event, see Takahashi et al. 2001), an additional scalar meson σ^* can be included, leading to a $\sigma\omega\rho\phi\sigma^*$ model. For the general $\sigma\omega\rho\phi\sigma^*$ model Lagrangian that includes quartic terms in vector-meson fields we develop a calculational scheme for the f_1^{ij} Landau Fermi-liquid parameters, and associated with them matrix Y_{ij}, as well as for the f_0^{ij} Landau parameters needed for calculation of various thermodynamic derivatives. Numerical calculations of f_0^{ij}, f_1^{ij} and Y_{ij} are done for three selected models of dense NH matter consistent with existence of 2 M$_\odot$ pulsars as well as with semi-empirical nuclear matter parameters at saturation, and semi-empirical hypernuclear data. For these models we also present EOS, Landau effective masses of baryons, and adiabatic indices. This data provide all microphysics input allowing one to model dynamics of superfluid NSs. All numerical results are available on-line.

The plan of this paper is as follows. Basic definitions and relations for superfluid NH mixture are recapitulated in Sect. 2. The $\sigma\omega\rho\phi\sigma^*$ Lagrangian for the baryon octet is presented in Sect. 3.1. The Dirac equations for baryons and their solutions in the RMF approximations are given in Sect. 3.2. The equations for the meson fields in the presence of baryon currents are given in Sect. 3.3. Sect. 3.4 presents expressions for thermodynamic functions. Landau parameters f_1^{ij} and f_0^{ij} are derived in Sect. 4 and 5, respectively. Numerical results are collected in Sect. 6. Three up-to-date RMF models of NH matter are presented in Sect. 6.1. The EOSs for these models as well as the parameters of NS configurations with maximum mass $M_{\rm max}$ are compared in the same Sect. 6.1. Particle fractions for NH matter in beta equilibrium, adiabatic indices, and the speed of sound, all as functions of baryon number density, are compared in Sect. 6.2. Landau effective masses are calculated in Sect. 6.3. Numerical results for the Landau Fermi-liquid parameters and entrainment matrix are presented in Sect. 6.4. Stability of the ground state of NH matter is briefly discussed in Sect. 6.5. Section 7 contains summary of our results. Detailed information about the coupling constants for the three RMF models employed in this paper is given in Appendix A. The way of calculating EOSs for these three models is reviewed in Appendix B. Adiabatic indices are discussed in Appendix C. Finally, a description of publicly available on-line numerical material containing the results of our calculations is given in Appendix D.

2 BASIC DEFINITIONS AND RELATIONS

Here we briefly review the Landau Fermi-liquid theory (see, e.g., Baym & Pethick 1991; Pines & Nozieres 1999) generalized to the case of relativistic one-component liquid by Baym & Chin (1976) and extended to relativistic mixtures by Gusakov et al. (2009b). For the sake of compactness of notation we use the convention $\hbar = c = 1$, where $\hbar$ is the Planck constant and c is the speed of light; we also assume that the metric tensor is $\eta_{\mu\nu} = {\rm diag}(1, -1, -1, -1)$. Unless otherwise stated, all quantities and relations are given in the reference system associated with normal fluid of leptons. In this reference system, the four-velocity of the normal fluid is $u^\mu = (1, 0, 0, 0)$.

We are dealing with an uniform mixture of baryon species. Let us first assume that all baryon species are *normal* (no superfluid gaps). This means that if we start with a (reference) system of bare noninteracting baryons and then the interaction is slowly switched on, the system of bare noninteracting baryons transforms adiabatically into a system of *Landau quasiparticles*. This system of quasiparticles retains essential properties of a mixture of ideal Fermi gases. Namely the distribution function of quasiparticles in the momentum space is the same as that of an ideal 'reference' system. The number of quasiparticles is equal to the number of particles. The Landau Fermi-liquid theory establishes therefore a one to one correspondence between

the states of a system of quasiparticles and those of the real system. The quasiparticle states will be labelled by momentum $\boldsymbol{p}$ and spin s, $\boldsymbol{p}s$. As we will deal with spin unpolarized systems, the quantities under consideration are spin independent and can be replaced by spin-averaged ones.

In the ground state, distribution function of quasiparticle species i is then a filled Fermi sphere,

$$n_{i0}(\boldsymbol{p}) = \theta(p_{\rm Fi} - p), \tag{1}$$

where $p_{\rm Fi}$ is the Fermi momentum for quasiparticles, coinciding with that for bare noninteracting particles, so that the number density $n_i = p_{\rm Fi}^3/3\pi^2$. $\theta(x)$ is the step function: $\theta(x) = 1$, if $x > 0$ and 0 otherwise. Subscript 0 will denote the quantities in the ground state of the system.

Within the normal Landau Fermi-liquid theory, the energy of the system is a functional of the quasiparticle distribution functions, $n_i(\boldsymbol{p})$. The validity of the quasiparticle description of an excited state is restricted to vicinity of the Fermi surfaces. This means, that $\delta n_i(\boldsymbol{p}) = n_i(\boldsymbol{p}) - n_{i0}(\boldsymbol{p})$ is nonzero for $|p - p_{\rm Fi}| \ll p_{\rm Fi}$. The energy E of an excited state of the system can be expressed in terms of $\delta n_i(\boldsymbol{p})$ by expanding the functional $E\{n_i(\boldsymbol{p})\}$ around E_0 (see, e.g., Baym & Pethick 1991; Pines & Nozieres 1999),

$$E - E_0 = \sum_{\boldsymbol{p}si} \varepsilon_{i0}(\boldsymbol{p})\, \delta n_i(\boldsymbol{p}) + \frac{1}{2} \sum_{\boldsymbol{p}\boldsymbol{p}'\, ss'\, ij} f^{ij}(\boldsymbol{p},\boldsymbol{p}')\, \delta n_i(\boldsymbol{p}) \delta n_j(\boldsymbol{p}') \ , \tag{2}$$

where third order terms in $\delta n_i(\boldsymbol{p})$ have been neglected. Here, $\varepsilon_{i0}(\boldsymbol{p})$ and $f^{ij}(\boldsymbol{p},\boldsymbol{p}')$ are, respectively, energy of a i-quasiparticle in the ground state, and the (spin-averaged) quasiparticle interaction – a central object in the Landau Fermi-liquid theory. Because of the isotropy of the ground state, $\varepsilon_{i0}(\boldsymbol{p})$ depends only on $|\boldsymbol{p}| = p$. This needs not to be so for a quasiparticle in an excited state of the system; in the latter case the quasiparticle energy is given by (Baym & Pethick 1991; Pines & Nozieres 1999)

$$\varepsilon_i(\boldsymbol{p}) = \varepsilon_{i0}(p) + \sum_{\boldsymbol{p}'s'j} f^{ij}(\boldsymbol{p},\boldsymbol{p}')\, \delta n_j(\boldsymbol{p}') \ . \tag{3}$$

Near the Fermi surface, the function $\varepsilon_{i0}(p)$ can be expanded into a series in powers of the quantity $p - p_{\rm Fi}$ and approximated by a linear form,

$$\varepsilon_{i0}(p) \approx \mu_i + v_{\rm Fi}(p - p_{\rm Fi}), \tag{4}$$

where $\mu_i = \varepsilon_{i0}(p_{\rm Fi})$ is the relativistic (i.e., including the rest energy) chemical potential or, equivalently, the Fermi energy of quasiparticle species i and $v_{{\rm F}i} = [\partial\varepsilon_{i0}(p)/\partial p]_{p=p_{\rm Fi}}$ is the velocity of quasiparticles on the Fermi surface. The Landau quasiparticle effective mass m_i^* is introduced through the relation

$$v_{\rm Fi} \equiv p_{\rm Fi}/m_i^* \ . \tag{5}$$

Within the region of validity of the Landau Fermi-liquid theory, the magnitude of momentum arguments of the quasiparticle interaction $f^{ij}(\boldsymbol{p},\boldsymbol{p}')$ can be approximated as $|\boldsymbol{p}| \approx p_{\rm Fi}$ and $|\boldsymbol{p}'| \approx p_{\rm Fj}$, respectively. Therefore, the momentum dependence of f^{ij} can be expanded into Legendre polynomials $P_\ell(\cos\theta)$,

$$f^{ij}(\boldsymbol{p},\boldsymbol{p}') = \sum_\ell f_\ell^{ij}\, P_\ell(\cos\theta), \tag{6}$$

where θ is the angle between $\boldsymbol{p}$ and $\boldsymbol{p}'$ and f_ℓ^{ij} are the Landau Fermi-liquid parameters, $f_\ell^{ij} = f_\ell^{ji}$. The dimensionless Landau parameters F_ℓ^{ij} are defined through

$$F_\ell^{ij} \equiv \sqrt{N_{{\rm F}i} N_{{\rm F}j}}\, f_\ell^{ij} \ , \ N_{{\rm F}i} = m_i^* p_{{\rm F}i}/\pi^2 \ , \tag{7}$$

where $N_{{\rm F}i}$ is the density of i-quasiparticle states at the Fermi surface.

The effective mass m_i^* in the relativistic theory can be expressed in terms of the Landau parameters F_1^{ij} [see equation (24) of Gusakov et al. 2009b],

$$\frac{\mu_i}{m_i^*} = 1 - \frac{1}{3} \sum_j \frac{\mu_j}{\sqrt{m_i^* m_j^*}} \left(\frac{p_{{\rm F}j}}{p_{{\rm F}i}}\right)^{3/2} F_1^{ij}. \tag{8}$$

Let us pass now to the *superfluid baryons*. A mixture of baryon superfluids is described in terms of *Bogoliubov quasiparticles*. At $T = 0$ all baryons are paired into Cooper pairs and the energy gaps for (Bogoliubov) i-quasiparticles at the Fermi surface are Δ_i (for the sake of simplicity we restrict ourselves to isotropic gaps). As long as $\Delta_i \ll \mu_i - m_i$, the energy gaps will not affect the main formulas, e.g., the particle current densities $\boldsymbol{j}_i$ will be related to the distribution functions by the same expression as in the case of a normal Fermi liquid, see Leggett (1965, 1975).

We consider excited states of the system associated with uniform superfluid flows, each of them with macroscopic velocity $\boldsymbol{V}_{{\rm s}i}$. The macroscopic flow velocity of species i is related to the total momentum of a Cooper pair $2\boldsymbol{Q}_i$ by

$$\boldsymbol{V}_{{\rm s}i} = \frac{\boldsymbol{Q}_i}{m_i}, \tag{9}$$

where m_i is a free (in vacuum) mass of baryon i. In the linear approximation in $\boldsymbol{Q}_i$ ($|\boldsymbol{Q}_i| \ll p_{\mathrm{F}i}$), the current densities $\boldsymbol{j}_i$ are connected with $\{\boldsymbol{Q}_j\}$ by (Gusakov et al. 2009b)

$$\boldsymbol{j}_i = \sum_j Y_{ij}\,\boldsymbol{Q}_j. \tag{10}$$

The relativistic entrainment matrix, Y_{ij}, is symmetric, $Y_{ij} = Y_{ji}$, and fulfils a sum rule

$$\sum_j \mu_j\, Y_{ij} = n_i\ . \tag{11}$$

In the case of vanishing temperature ($T = 0$), the entrainment matrix can be expressed in terms of the F_1^{ij} Landau parameters (Gusakov et al. 2009b),

$$Y_{ij} = \frac{n_i}{m_i^*}\delta_{ij} + \frac{1}{3}\left(\frac{n_i n_j}{m_i^* m_j^*}\right)^{1/2} F_1^{ij}\ , \tag{12}$$

where δ_{ij} is the Kronecker delta. The non-diagonal elements of Y_{ij} describe the superfluid entrainment, a non-dissipative interaction between the superfluid baryon flows.

The more complex expression for Y_{ij}, valid at arbitrary temperature, was formulated by Gusakov et al. (2009a). It also involves the Landau parameters F_1^{ij} (see Eqs. (41)–(43) and (45) of that reference).

3 THE $\sigma\omega\rho\phi\sigma^*$ MODEL

We use a nonlinear model of Bednarek & Manka (2009).

3.1 Lagrangian

The Lagrangian density $\mathcal{L}$ of the strongly interacting baryon system can be split into two basic components, $\mathcal{L}_{\mathrm{BM}}$ involving baryon terms affected by the meson fields, and $\mathcal{L}_{\mathrm{M}}$ involving exclusively meson fields.

We consider Dirac spinor fields for baryons Ψ_i, depending on spacetime point x. The contravariant coordinates of x are $x^\mu = (x^0, x^1, x^2, x^3, x^4)$, and the contravariant derivative $\partial^\mu = \partial/\partial x_\mu$. The $\mathcal{L}_{\mathrm{BM}}$ component of the Lagrangian density is then

$$\mathcal{L}_{\mathrm{BM}} = \sum_i \overline{\Psi}_i \left(\mathrm{i}\gamma_\mu\partial^\mu - m_i - g_{\omega i}\gamma_\mu\omega^\mu - g_{\phi i}\gamma_\mu\phi^\mu - \frac{1}{2}g_{\rho i}\tau_a\gamma_\mu\rho_a^\mu + g_{\sigma i}\sigma + g_{\sigma^* i}\sigma^*\right)\Psi_i\ , \tag{13}$$

where γ_μ are Dirac matrices and $\overline{\Psi}_i \equiv \Psi_i^\dagger\gamma_0$ is an adjoint Dirac spinor. The components of τ_a ($a = 1, 2, 3$) are Pauli matrices acting in the isospin space. The parameters g_{mi} ($m = \sigma$, σ^*, ω, ρ, ϕ) are coupling constants of the meson fields to the baryon fields.

Baryon densities and currents are sources of the meson fields. We assume spatially uniform and time independent sources and therefore resulting meson fields are x-independent. Meson fields and their interactions generate the meson Lagrangian $\mathcal{L}_{\mathrm{M}} = \mathcal{L}_{\mathrm{M}}^{(\mathrm{S})} + \mathcal{L}_{\mathrm{M}}^{(\mathrm{V})}$, where S and V refer to the scalar and vector mesons, respectively. The scalar meson contribution is

$$\mathcal{L}_{\mathrm{M}}^{(\mathrm{S})} = -\frac{1}{2}m_\sigma^2\sigma^2 - \frac{1}{2}m_{\sigma^*}^2\sigma^{*2} - \frac{1}{3}g_3\sigma^3 - \frac{1}{4}g_4\sigma^4, \tag{14}$$

where the coupling constants g_3 and g_4 determine the strength of σ meson self-interaction.

The vector meson contribution includes terms quadratic and quartic in vector meson fields,

$$\begin{aligned}\mathcal{L}_{\mathrm{M}}^{(\mathrm{V})} \;=\;& \underline{\frac{1}{2}m_\omega^2(\omega_\mu\omega^\mu)} + \underline{\frac{1}{2}m_\rho^2(\rho_{a\mu}\rho_a^\mu)} + \underline{\frac{1}{2}m_\phi^2(\phi_\mu\phi^\mu)} + \underline{\frac{1}{4}c_3(\omega_\mu\omega^\mu)^2}\\
&+\frac{1}{4}\widetilde{c}_3(\rho_{a\mu}\rho_a^\mu)^2 + \frac{3}{4}\widetilde{c}_3(\rho_{a\mu}\rho_a^\mu)(\phi_\nu\phi^\nu) + \frac{1}{8}\widetilde{c}_3(\phi_\mu\phi^\mu)^2\\
&+\frac{3}{4}\widetilde{c}_3(\phi_\mu\phi^\mu)(\omega_\nu\omega^\nu) + \frac{1}{4}(g_{\rho\mathrm{N}}g_{\omega\mathrm{N}})^2\Lambda_{\mathrm{V}}(\phi_\mu\phi^\mu)^2 - \frac{1}{2}(g_{\rho\mathrm{N}}g_{\omega\mathrm{N}})^2\Lambda_{\mathrm{V}}(\rho_{a\mu}\rho_a^\mu)(\phi_\nu\phi^\nu)\\
&+(g_{\rho\mathrm{N}}g_{\omega\mathrm{N}})^2\Lambda_{\mathrm{V}}(\rho_{a\mu}\rho_a^\mu)(\omega_\nu\omega^\nu) - \frac{1}{2}(g_{\rho\mathrm{N}}g_{\omega\mathrm{N}})^2\Lambda_{\mathrm{V}}(\phi_\mu\phi^\mu)(\omega_\nu\omega^\nu).\end{aligned} \tag{15}$$

In Eqs. (14) and (15) m_σ, m_{σ^*}, m_ω, m_ρ, and m_ϕ are the corresponding meson masses. Three additional parameters in Eq. (15), c_3, $\widetilde{c}_3$, and Λ_{V}, determine the strength of the quartic vector meson terms. (Notice that in Bednarek & Manka 2009 it was assumed that $\widetilde{c}_3 = c_3$.) For less general models considered by us in Sect. 6 only the underlined terms in Eq. (15) are taken into account, that is we put $\widetilde{c}_3 = \Lambda_{\mathrm{V}} = 0$.

3.2 The microscopic state of baryons in the RMF approximation

The equations of motion for the baryon fields Ψ_i are obtained as Euler-Lagrange equations from $\mathcal{L}$,

$$\partial\mathcal{L}/\partial\overline{\Psi}_i = \left(\mathrm{i}\gamma_\mu\partial^\mu - m_i - g_{\omega i}\gamma_\mu\omega^\mu - g_{\phi i}\gamma_\mu\phi^\mu - \frac{1}{2}g_{\rho i}\tau_a\gamma_\mu\rho_a^\mu + g_{\sigma i}\sigma + g_{\sigma^* i}\sigma^*\right)\Psi_i = 0\ . \tag{16}$$

These are Dirac equations for baryons coupled to meson fields. We look for the macroscopic states of NH matter which are uniform in space and stationary. In the RMF approximation, the meson fields in $\mathcal{L}$ are replaced by their x-independent mean values. Therefore, solutions Ψ_i of Eq. (16) are the eigenstates of the four-momentum p^μ,

$$\Psi_i = \Psi_i(p^\mu)\mathrm{e}^{-\mathrm{i}p^\mu x_\mu}\ . \tag{17}$$

After putting Ansatz (17) into the equation of motion (16), we solve it using standard methods for the Dirac equation. In this way we find the *Dirac equation eigenvalues* of the energy, e_i, at fixed values of the uniform meson fields,

$$\begin{aligned} e_i(\boldsymbol{p}) &= g_{\omega i}\omega^0 + g_{\rho i}I_{3i}\rho_3^0 + g_{\phi i}\phi^0 \\ &+ \left[(\boldsymbol{p} - g_{\omega i}\boldsymbol{\omega} - g_{\rho i}I_{3i}\boldsymbol{\rho}_3 - g_{\phi i}\boldsymbol{\phi})^2 + (m_i - g_{\sigma i}\sigma - g_{\sigma^* i}\sigma^*)^2\right]^{1/2}, \end{aligned} \tag{18}$$

where I_{3i} is the third component of the isospin of baryon i, with $I_{3\mathrm{n}} = -1/2$ (the subscript n stands for neutrons).

A macroscopic spatially uniform stationary state for baryons, under given constraints on baryon currents, $\boldsymbol{j}_i$, and baryon densities, n_i, is obtained by filling lowest Dirac energy eigenstates. The distribution function of the occupied Dirac states coincides then with distribution function of the Landau i-quasiparticles. Therefore, in the RMF approximation, the quasiparticle energy of a baryon species i is equal to the Dirac equation eigenvalue, $\varepsilon_i(\boldsymbol{p}) = e_i(\boldsymbol{p})$. In particular, the particle current density can be expressed through $e_i(\boldsymbol{p})$ as

$$\boldsymbol{j}_i = \sum_{\boldsymbol{p}s}\frac{\partial e_i(\boldsymbol{p})}{\partial\boldsymbol{p}}\,n_i(\boldsymbol{p}). \tag{19}$$

3.3 Field equations for meson fields in the presence of baryon currents

Meson fields are calculated assuming a uniform stationary state of baryons. The field equations for mesons are the Euler-Lagrange equations obtained from $\mathcal{L}$. The baryon fields enter the source terms in the meson field equation. In the RMF approximation, the source term is replaced by a mean value calculated in the uniform stationary state of the baryon system described in Sect. 3.2. Both source terms and meson fields are x-independent. Equations for meson fields can be written as

$$m_\sigma^2\,\sigma = -g_3\,\sigma^2 - g_4\,\sigma^3 + \sum_i g_{\sigma i}\,R_i(m_i - g_{\sigma i}\,\sigma - g_{\sigma^* i}\,\sigma^*,\ g_{\omega i}\,\boldsymbol{\omega} + g_{\rho i}\,I_{3i}\,\boldsymbol{\rho}_3 + g_{\phi i}\,\boldsymbol{\phi}), \tag{20}$$

$$m_{\sigma^*}^2\,\sigma^* = \sum_i g_{\sigma^* i}\,R_i(m_i - g_{\sigma i}\,\sigma - g_{\sigma^* i}\,\sigma^*,\ g_{\omega i}\,\boldsymbol{\omega} + g_{\rho i}\,I_{3i}\,\boldsymbol{\rho}_3 + g_{\phi i}\,\boldsymbol{\phi}), \tag{21}$$

$$\left[m_\omega^2 + A_\omega\,(\omega_\nu\omega^\nu) + A_\rho\,(\rho_{3\,\nu}\rho_3^\nu) + A_\phi\,(\phi_\nu\phi^\nu)\right]\,\omega^\mu = \sum_i g_{\omega i}\,j_i^\mu, \tag{22}$$

$$\left[m_\rho^2 + B_\omega\,(\omega_\nu\omega^\nu) + B_\rho\,(\rho_{3\,\nu}\rho_3^\nu) + B_\phi\,(\phi_\nu\phi^\nu)\right]\,\rho_3^\mu = \sum_i g_{\rho i}\,I_{3i}\,j_i^\mu, \tag{23}$$

$$\left[m_\phi^2 + C_\omega\,(\omega_\nu\omega^\nu) + C_\rho\,(\rho_{3\,\nu}\rho_3^\nu) + C_\phi\,(\phi_\nu\phi^\nu)\right]\,\phi^\mu = \sum_i g_{\phi i}\,j_i^\mu. \tag{24}$$

Here

$$R_i(x,\boldsymbol{y}) = \sum_{\boldsymbol{p}s}\frac{x}{\sqrt{(\boldsymbol{p}-\boldsymbol{y})^2 + x^2}}\,n_i(\boldsymbol{p}). \tag{25}$$

In case of the $\sigma\omega\rho\phi\sigma^*$ Lagrangian of Bednarek & Manka (2009), described in Sect. 3.1, the constants $A_\omega,\ldots,C_\phi$ in Eqs. (22)–(24) are given by expressions

$$A_\omega = c_3,\quad A_\rho = 2\,\Lambda_\mathrm{V}\,(g_{\omega\mathrm{N}}g_{\rho\mathrm{N}})^2,\quad A_\phi = \frac{3}{2}\widetilde{c}_3 - \Lambda_\mathrm{V}\,(g_{\omega\mathrm{N}}g_{\rho\mathrm{N}})^2, \tag{26}$$

$$B_\omega = 2\,\Lambda_\mathrm{V}\,(g_{\omega\mathrm{N}}g_{\rho\mathrm{N}})^2,\quad B_\rho = \widetilde{c}_3,\quad B_\phi = A_\phi, \tag{27}$$

$$C_\omega = \frac{3}{2}\widetilde{c}_3 - \Lambda_\mathrm{V}\,(g_{\omega\mathrm{N}}g_{\rho\mathrm{N}})^2,\quad C_\rho = C_\omega,\quad C_\phi = \frac{1}{2}\widetilde{c}_3 + \Lambda_\mathrm{V}\,(g_{\omega\mathrm{N}}g_{\rho\mathrm{N}})^2. \tag{28}$$

As we already emphasized above, for less general RMF models considered in Sect. 6, the only non-zero constant is $A_\omega = c_3$ ($\widetilde{c}_3 = \Lambda_\mathrm{V} = 0$). Neglecting σ^* and ϕ mesons, Eqs. (20)–(28) correctly reproduce the $\sigma\omega\rho$ model of Glendenning (Glendenning 2000; Gusakov et al. 2009b).

3.4 Chemical potential, energy density, and pressure

In this section, we assume that there is no baryon currents in the system, that is, $\boldsymbol{w} = \boldsymbol{\rho}_3 = \boldsymbol{\phi} = 0$. Knowledge of the particle energy (18) allows one to immediately find the relativistic chemical potential μ_i,

$$\mu_i = e_i(p_{\mathrm{F}i}) = g_{\omega i}\omega^0 + g_{\rho i} I_{3i}\rho_3^0 + g_{\phi i}\phi^0 + \sqrt{p_{\mathrm{F}i}^2 + (m_i - g_{\sigma i}\sigma - g_{\sigma^* i}\sigma^*)^2} \tag{29}$$

and the Landau effective mass m_i^* (cf. equation (47) of Gusakov et al. 2009b),

$$m_i^* = \frac{p_{\mathrm{F}i}}{|\partial e_i(\boldsymbol{p})/\partial \boldsymbol{p}|_{p=p_{\mathrm{F}i}}} = \sqrt{p_{\mathrm{F}i}^2 + (m_i - g_{\sigma i}\sigma - g_{\sigma^* i}\sigma^*)^2}. \tag{30}$$

The energy density ρ (also termed *density* in what follows) can be obtained from the Lagrangian of Sect. 3.1 in the same way as it was done, e.g., in Glendenning (2000). The result is

$$\begin{aligned}\rho = & - \langle\mathcal{L}\rangle + \sum_i \left[g_{\omega i}\,\omega^0\,n_i + g_{\rho i} I_{3i}\,\rho_3^0\,n_i + g_{\phi i}\,\phi^0\,n_i + R_{\mathrm{E}}(m_i - g_{\sigma i}\,\sigma - g_{\sigma^* i}\,\sigma^*,\ p_{\mathrm{F}i})\right] \\ & + \sum_{l=\mathrm{e},\,\mu} R_{\mathrm{E}}(m_l,\ p_{\mathrm{F}l}),\end{aligned} \tag{31}$$

where the summation is performed over all baryon species i and lepton species $l = \mathrm{e},\ \mu$;

$$\begin{aligned}\langle\mathcal{L}\rangle = & -\frac{1}{2}m_\sigma^2\sigma^2 - \frac{1}{3}g_3\sigma^3 - \frac{1}{4}g_4\sigma^4 + \frac{1}{2}m_\omega^2(\omega^0)^2 + \frac{1}{2}m_\rho^2(\rho_3^0)^2 + \frac{1}{2}m_\phi^2(\phi^0)^2 - \frac{1}{2}m_{\sigma^*}^2\sigma^{*2} \\ & + \frac{1}{4}c_3\,(\omega^0)^4 + \Lambda_{\mathrm{V}}\,(g_{\omega\mathrm{N}}g_{\rho\mathrm{N}})^2\,(\omega^0)^2(\rho_3^0)^2 - \left[\frac{1}{2}\Lambda_{\mathrm{V}}\,(g_{\omega\mathrm{N}}g_{\rho\mathrm{N}})^2 - \frac{3}{4}\widetilde{c}_3\right](\omega^0)^2(\phi^0)^2 \\ & - \left[\frac{1}{2}\Lambda_{\mathrm{V}}\,(g_{\omega\mathrm{N}}g_{\rho\mathrm{N}})^2 - \frac{3}{4}\widetilde{c}_3\right](\rho_3^0)^2(\phi^0)^2 + \frac{1}{4}\widetilde{c}_3(\rho_3^0)^4 + \left[\frac{1}{4}\Lambda_{\mathrm{V}}\,(g_{\omega\mathrm{N}}g_{\rho\mathrm{N}})^2 + \frac{1}{8}\widetilde{c}_3\right](\phi^0)^4,\end{aligned} \tag{32}$$

and

$$R_{\mathrm{E}}(x,\,y) = \frac{1}{\pi^2}\int_0^y p^2\,\sqrt{p^2 + x^2}\,\mathrm{d}p. \tag{33}$$

Now the pressure P can be expressed through ρ and μ_k by the following standard formula,

$$P = -\rho + \sum_k \mu_k n_k, \tag{34}$$

where the subscript k runs over all particle species (baryons and leptons).

4 DERIVATION OF EXPRESSION FOR f_1^{ij}

To calculate the Landau parameter f_1^{ij} we have to create a uniform baryon current in the system. For that we shift the distribution function $n_{i0}(\boldsymbol{p})$ (the step function) of a baryon species i by a small vector $\boldsymbol{Q}_i$. Note that, in the linear approximation in $\boldsymbol{Q}_i$, the scalars σ, σ^*, $\omega_\mu\omega^\mu$, $\rho_{3\,\mu}\rho_3^\mu$, and $\phi_\mu\phi^\mu$ remain the same as in the absence of baryon currents.

Following the derivation of equation (43) of Gusakov et al. (2009b), one obtains

$$\boldsymbol{\jmath}_i = \frac{n_i}{m_i^*}\,\left(\boldsymbol{Q}_i - g_{\omega i}\,\boldsymbol{\omega} - g_{\rho i}\,I_{3i}\,\boldsymbol{\rho}_3 - g_{\phi i}\,\boldsymbol{\phi}\right), \tag{35}$$

where m_i^* is given by Eq. (30). Eq. (35) should be supplemented by the expressions for $\boldsymbol{\omega}$, $\boldsymbol{\rho}_3$, and $\boldsymbol{\phi}$. These expressions can be found from Eqs. (22)–(24),

$$m_\omega^{*2}\,\boldsymbol{\omega} = \sum_i g_{\omega i}\,\boldsymbol{\jmath}_i, \tag{36}$$

$$m_\rho^{*2}\,\boldsymbol{\rho}_3 = \sum_i g_{\rho i}\,I_{3i}\,\boldsymbol{\jmath}_i, \tag{37}$$

$$m_\phi^{*2}\,\boldsymbol{\phi} = \sum_i g_{\phi i}\,\boldsymbol{\jmath}_i, \tag{38}$$

where we defined the effective meson masses

$$m_\omega^{*2} = m_\omega^2 + A_\omega\,(\omega^0)^2 + A_\rho\,(\rho_3^0)^2 + A_\phi\,(\phi^0)^2, \tag{39}$$

$$m_\rho^{*2} = m_\rho^2 + B_\omega\,(\omega^0)^2 + B_\rho\,(\rho_3^0)^2 + B_\phi\,(\phi^0)^2, \tag{40}$$

$$m_\phi^{*2} = m_\phi^2 + C_\omega\,(\omega^0)^2 + C_\rho\,(\rho_3^0)^2 + C_\phi\,(\phi^0)^2, \tag{41}$$

and made use of the fact that, for example, $\omega_\mu\omega^\mu = (\omega^0)^2$ with the accuracy to linear terms in $\boldsymbol{Q}_i$ (ω^0 is also independent of $\boldsymbol{Q}_i$ in the linear approximation).

Eq. (35) should be solved together with Eqs. (36)–(38). To proceed further, let us multiply (35) by $g_{\omega i}$ and sum it over i. Then, using Eq. (36), one obtains

$$m_\omega^{*2}\,\boldsymbol{\omega} = \sum_i \frac{n_i}{m_i^*}\,g_{\omega i}\,\left(\boldsymbol{Q}_i - g_{\omega i}\,\boldsymbol{\omega} - g_{\rho i}\,I_{3i}\,\boldsymbol{\rho}_3 - g_{\phi i}\,\boldsymbol{\phi}\right). \tag{42}$$

Similarly,

$$m_\rho^{*2}\,\boldsymbol{\rho}_3 = \sum_i \frac{n_i}{m_i^*}\,g_{\rho i}\,I_{3i}\,\left(\boldsymbol{Q}_i - g_{\omega i}\,\boldsymbol{\omega} - g_{\rho i}\,I_{3i}\,\boldsymbol{\rho}_3 - g_{\phi i}\,\boldsymbol{\phi}\right), \tag{43}$$

$$m_\phi^{*2}\,\boldsymbol{\phi} = \sum_i \frac{n_i}{m_i^*}\,g_{\phi i}\,\left(\boldsymbol{Q}_i - g_{\omega i}\,\boldsymbol{\omega} - g_{\rho i}\,I_{3i}\,\boldsymbol{\rho}_3 - g_{\phi i}\,\boldsymbol{\phi}\right). \tag{44}$$

Eqs. (42)–(44) can be rewritten in the matrix form,

$$\left(\begin{array}{ccc} m_\omega^{*2}+\sum_i \frac{n_i}{m_i^*}\,g_{\omega i}^2 & \sum_i \frac{n_i}{m_i^*}\,g_{\omega i}\,g_{\rho i}\,I_{3i} & \sum_i \frac{n_i}{m_i^*}\,g_{\omega i}\,g_{\phi i} \\ \sum_i \frac{n_i}{m_i^*}\,g_{\omega i}\,g_{\rho i}\,I_{3i} & m_\rho^{*2}+\sum_i \frac{n_i}{m_i^*}\,g_{\rho i}^2\,I_{3i}^2 & \sum_i \frac{n_i}{m_i^*}\,g_{\rho i}\,I_{3i}\,g_{\phi i} \\ \sum_i \frac{n_i}{m_i^*}\,g_{\omega i}\,g_{\phi i} & \sum_i \frac{n_i}{m_i^*}\,g_{\rho i}\,I_{3i}\,g_{\phi i} & m_\phi^{*2}+\sum_i \frac{n_i}{m_i^*}\,g_{\phi i}^2 \end{array}\right) \left(\begin{array}{c} \boldsymbol{\omega} \\ \boldsymbol{\rho}_3 \\ \boldsymbol{\phi} \end{array}\right) = \left(\begin{array}{c} \sum_i \frac{n_i}{m_i^*}\,g_{\omega i}\,\boldsymbol{Q}_i \\ \sum_i \frac{n_i}{m_i^*}\,g_{\rho i}\,I_{3i}\,\boldsymbol{Q}_i \\ \sum_i \frac{n_i}{m_i^*}\,g_{\phi i}\,\boldsymbol{Q}_i \end{array}\right). \tag{45}$$

The solution to Eq. (45) can be presented as

$$\boldsymbol{\omega} = \sum_j \alpha_{\omega j}\,\boldsymbol{Q}_j, \tag{46}$$

$$\boldsymbol{\rho}_3 = \sum_j \alpha_{\rho j}\,\boldsymbol{Q}_j, \tag{47}$$

$$\boldsymbol{\phi} = \sum_j \alpha_{\phi j}\,\boldsymbol{Q}_j, \tag{48}$$

where the coefficients $\alpha_{\omega j}$, $\alpha_{\rho j}$, and $\alpha_{\phi j}$ can be determined from Eq. (45) using the methods of linear algebra. Using Eqs. (35) and (46)–(48), one can calculate the entrainment matrix Y_{ij},

$$Y_{ij} = \frac{n_i}{m_i^*}\left(\delta_{ij} - g_{\omega i}\,\alpha_{\omega j} - g_{\rho i}\,I_{3i}\,\alpha_{\rho j} - g_{\phi i}\,\alpha_{\phi j}\right), \tag{49}$$

and, consequently, the Landau parameters f_1^{ij} [see equation (46) of Gusakov et al. 2009b or Eq. (12)].

5 DERIVATION OF EXPRESSION FOR f_0^{ij}

Here we will closely follow the derivation of section IIIC in Gusakov et al. (2009b). Let us consider a system without baryon currents (i.e., $\boldsymbol{\omega} = \boldsymbol{\rho}_3 = \boldsymbol{\phi} = 0$). To calculate the Landau parameters f_0^{ij} we slightly vary the Fermi momentum $p_{\mathrm{F}i}$ by a small quantity $\Delta p_{\mathrm{F}i}$, so that the distribution function of a quasiparticle species i will become $n_i(\boldsymbol{p}) = \theta(p_{\mathrm{F}i} + \Delta p_{\mathrm{F}i} - p)$. This will shift the energy of baryons $e_i(\boldsymbol{p})$ by a small quantity $\delta e_i(\boldsymbol{p})$. At $p = p_{\mathrm{F}i}$ the expression for $\delta e_i(\boldsymbol{p})$ takes the form [see Eq. (18)]

$$\begin{aligned}\delta e_i(p_{\mathrm{F}i}) &= g_{\omega i}\,\delta\omega^0 + g_{\rho i}\,I_{3i}\,\delta\rho_3^0 + g_{\phi i}\,\delta\phi^0 \\ &- (m_i/m_i^* - g_{\sigma i}\,\sigma/m_i^* - g_{\sigma^* i}\,\sigma^*/m_i^*)\,(g_{\sigma i}\,\delta\sigma + g_{\sigma^* i}\,\delta\sigma^*),\end{aligned} \tag{50}$$

where we used Eq. (30) for the Landau effective mass m_i^*. On the other hand, it follows from the Landau theory of Fermi liquids that

$$\delta e_i(p_{\mathrm{F}i}) = \sum_j f_0^{ij}\,\delta n_j, \tag{51}$$

where $\delta n_j \equiv p_{\mathrm{F}j}^2 \Delta p_{\mathrm{F}j}/\pi^2$. Comparing Eqs. (50) and (51) one can calculate the parameters f_0^{ij}. For that we need to express the variations $\delta\sigma$, $\delta\sigma^*$, $\delta\omega^0$, $\delta\rho_3^0$, and $\delta\phi^0$ through δn_i. We start with the quantities $\delta\sigma$ and $\delta\sigma^*$. They can be found from the linearized Eqs. (20) and (21),

$$\begin{aligned}(m_\sigma^2 + 2\,g_3\,\sigma + 3\,g_4\,\sigma^2)\,\delta\sigma = &-\sum_i g_{\sigma i}\,\frac{\partial R_i(x,0)}{\partial x}|_{x=m_i - g_{\sigma i}\,\sigma - g_{\sigma^* i}\,\sigma^*}\,(g_{\sigma i}\,\delta\sigma + g_{\sigma^* i}\,\delta\sigma^*) \\ &+ \sum_i g_{\sigma i}\,(m_i/m_i^* - g_{\sigma i}\,\sigma/m_i^* - g_{\sigma^* i}\,\sigma^*/m_i^*)\,\delta n_i,\end{aligned} \tag{52}$$

$$\begin{aligned}m_{\sigma^*}^2\,\delta\sigma^* = &-\sum_i g_{\sigma^* i}\,\frac{\partial R_i(x,0)}{\partial x}|_{x=m_i - g_{\sigma i}\,\sigma - g_{\sigma^* i}\,\sigma^*}\,(g_{\sigma i}\,\delta\sigma + g_{\sigma^* i}\,\delta\sigma^*) \\ &+ \sum_i g_{\sigma^* i}\,(m_i/m_i^* - g_{\sigma i}\,\sigma/m_i^* - g_{\sigma^* i}\,\sigma^*/m_i^*)\,\delta n_i.\end{aligned} \tag{53}$$

In the matrix form Eqs. (52) and (53) can be rewritten as

$$\left(\begin{array}{cc} m_\sigma^2 + 2\,g_3\,\sigma + 3\,g_4\,\sigma^2 + I_{\sigma\sigma} & I_{\sigma\sigma^*} \\ I_{\sigma\sigma^*} & m_{\sigma^*}^2 + I_{\sigma^*\sigma^*} \end{array} \right) \left(\begin{array}{c} \delta\sigma \\ \delta\sigma^* \end{array} \right) =$$
$$= \left(\begin{array}{c} \sum_i g_{\sigma i}\,[m_i/m_i^* - g_{\sigma i}\,\sigma/m_i^* - g_{\sigma^* i}\,\sigma^*/m_i^*]\,\delta n_i \\ \sum_i g_{\sigma^* i}\,[m_i/m_i^* - g_{\sigma i}\,\sigma/m_i^* - g_{\sigma^* i}\,\sigma^*/m_i^*]\,\delta n_i \end{array} \right), \quad (54)$$

where we defined

$$I_{\sigma\sigma} = \sum_i g_{\sigma i}^2\,\frac{\partial R_i(x,0)}{\partial x}|_{x=m_i-g_{\sigma i}\,\sigma-g_{\sigma^* i}\,\sigma^*}, \quad (55)$$

$$I_{\sigma\sigma^*} = \sum_i g_{\sigma i}\,g_{\sigma^* i}\,\frac{\partial R_i(x,0)}{\partial x}|_{x=m_i-g_{\sigma i}\,\sigma-g_{\sigma^* i}\,\sigma^*}, \quad (56)$$

$$I_{\sigma^*\sigma^*} = \sum_i g_{\sigma^* i}^2\,\frac{\partial R_i(x,0)}{\partial x}|_{x=m_i-g_{\sigma i}\,\sigma-g_{\sigma^* i}\,\sigma^*}. \quad (57)$$

The solution to the system (54) can be easily found. To calculate the quantities $\delta\omega^0$, $\delta\rho^0$, and $\delta\phi^0$ we have to linearize the corresponding Eqs. (22)–(24). The result is

$$m_\omega^{*2}\,\delta\omega^0 + 2\left(A_\omega\,\omega^0\delta\omega^0 + A_\rho\,\rho_3^0\,\delta\rho_3^0 + A_\phi\,\phi^0\,\delta\phi^0\right)\,\omega^0 = \sum_i g_{\omega i}\,\delta n_i, \quad (58)$$

$$m_\rho^{*2}\,\delta\rho_3^0 + 2\left(B_\omega\,\omega^0\delta\omega^0 + B_\rho\,\rho_3^0\,\delta\rho_3^0 + B_\phi\,\phi^0\,\delta\phi^0\right)\,\rho_3^0 = \sum_i g_{\rho i}\,I_{3i}\,\delta n_i, \quad (59)$$

$$m_\phi^{*2}\,\delta\phi^0 + 2\left(C_\omega\,\omega^0\delta\omega^0 + C_\rho\,\rho_3^0\,\delta\rho_3^0 + C_\phi\,\phi^0\,\delta\phi^0\right)\,\phi^0 = \sum_i g_{\phi i}\,\delta n_i, \quad (60)$$

where the meson effective masses m_ω^*, m_ρ^*, and m_ϕ^* are given by Eqs. (39)–(41). In the matrix form the system of equations (58)–(60) is presented as

$$\left(\begin{array}{ccc} m_\omega^{*2} + 2\,A_\omega\,(\omega^0)^2 & 2\,A_\rho\,\omega^0\,\rho_3^0 & 2\,A_\phi\,\omega^0\,\phi^0 \\ 2\,B_\omega\,\omega^0\,\rho_3^0 & m_\rho^{*2} + 2\,B_\rho\,(\rho_3^0)^2 & 2\,B_\phi\,\rho_3^0\,\phi^0 \\ 2\,C_\omega\,\omega^0\,\phi^0 & 2\,C_\rho\,\rho_3^0\,\phi^0 & m_\phi^{*2} + 2\,C_\phi\,(\phi^0)^2 \end{array} \right) \left(\begin{array}{c} \delta\omega^0 \\ \delta\rho_3^0 \\ \delta\phi^0 \end{array} \right) = \left(\begin{array}{c} \sum_i g_{\omega i}\,\delta n_i \\ \sum_i g_{\rho i}\,I_{3i}\,\delta n_i \\ \sum_i g_{\phi i}\,\delta n_i \end{array} \right). \quad (61)$$

The solution to this matrix equation can also be easily obtained. Schematically, expressions for $\delta\sigma$, $\delta\sigma^*$, $\delta\omega^0$, $\delta\rho_3^0$, and $\delta\phi^0$ can be written as

$$\delta\sigma = \sum_j \beta_{\sigma j}\,\delta n_j, \quad (62)$$

$$\delta\sigma^* = \sum_j \beta_{\sigma^* j}\,\delta n_j, \quad (63)$$

$$\delta\omega^0 = \sum_j \beta_{\omega j}\,\delta n_j, \quad (64)$$

$$\delta\rho_3^0 = \sum_j \beta_{\rho j}\,\delta n_j, \quad (65)$$

$$\delta\phi^0 = \sum_j \beta_{\phi j}\,\delta n_j, \quad (66)$$

where we assume that the quantities $\beta_{\sigma j}, \ldots, \beta_{\phi j}$ have been already calculated from Eqs. (54) and (61). Finally, taking into account Eqs. (62)–(66) and comparing Eqs. (50) and (51), one finds the following expression for the Landau parameters f_0^{ij},

$$f_0^{ij} = g_{\omega i}\,\beta_{\omega j} + g_{\rho i}\,I_{3i}\,\beta_{\rho j} + g_{\phi i}\,\beta_{\phi j}$$
$$- (m_i/m_i^* - g_{\sigma i}\,\sigma/m_i^* - g_{\sigma^* i}\,\sigma^*/m_i^*)\,(g_{\sigma i}\,\beta_{\sigma j} + g_{\sigma^* i}\,\beta_{\sigma^* j}). \quad (67)$$

It can be shown (see, e.g., Gusakov et al. 2009b) that these parameters are directly related to the derivatives $\partial\mu_i/\partial n_j$, which should be taken at fixed particle number densities n_k ($k \neq j$). Namely, one has the following relation

$$\frac{\partial\mu_i(n_{\rm n}, \ldots, n_{\Sigma^+})}{\partial n_j} = \frac{\partial\mu_j(n_{\rm n}, \ldots, n_{\Sigma^+})}{\partial n_i} = f_0^{ij} + \frac{1}{N_{{\rm F}i}}\delta_{ij}, \quad (68)$$

where $N_{{\rm F}i}$ is defined by Eq. (7).

RMF model	$M_{\rm max}$ ($M_\odot$)	$R(M_{\rm max})$ (km)	$\rho_{\rm max}/10^{15}$ (g cm^{-3})	$n_{\rm b,max}$ (fm^{-3})	$-\left(y_{\rm S}\right)_{\rm c}$	$-\langle y_{\rm S}\rangle$
GM1A	1.994	12.05	2.00	0.923	0.607	0.143
GM1′B	2.015	11.45	2.28	1.018	0.671	0.181
TM1C	2.056	12.51	1.85	0.856	0.493	0.093

Table 1. Parameters of non-rotating NS models with maximum allowable mass. The columns are (from left to right): RMF model of NH matter, maximum stellar mass in units of the solar mass, corresponding radius of the star in km, central density in g cm^{-3}, central baryon number density in fm^{-3}, the ratio of (minus) strangeness number density S to baryon number density $n_{\rm b}$ [$y_{\rm S} = -S/n_{\rm b} = -(n_\Lambda + 2n_{\Xi^-} + 2n_{\Xi^0})/n_{\rm b}$] in the centre of the star, the same ratio but averaged over the whole star.

6 NUMERICAL RESULTS

6.1 RMF models, EOSs and $M_{\rm max}$

We consider three RMF models of NH matter (we will call them **GM1A**, **GM1′B** and **TM1C**), which are specific realizations of $\sigma\omega\rho\phi\sigma^*$ model of Bednarek & Manka (2009). The parameters of the models are given in the Appendix A. Below we give their brief characteristics. For all the models the binding energy per nucleon at saturation is $B_{\rm s} = -16.3$ MeV. Moreover, they all reproduce the semi-empirical depths of potential wells for hyperons at rest in symmetric nuclear matter at saturation density, $U_\Lambda^{\rm (N)} = -28$ MeV , $U_\Xi^{\rm (N)} = -18$ MeV , $U_\Sigma^{\rm (N)} = 30$ MeV (e.g., Millener, Dover & Gal 1988). The parameters of NS configuration with $M_{\rm max}$ for non-rotating NS models are given in Table 1 for **GM1A**, **GM1′B** and **TM1C** models.

GM1A. In the nucleon sector this is the **GM1** model of Glendenning & Moszkowski (1991). The saturation baryon number density for this model $n_{\rm s} = 0.153$ fm^{-3}. Nuclear matter incompressibility at the saturation point, $K_{\rm s} = 300$ MeV, is somewhat larger than the semi-empirical estimates of this quantity. The symmetry energy $E_{\rm sym} = 32.5$ MeV is within the semi-empirical evaluations. The *Dirac effective nucleon mass* in symmetric nuclear matter at saturation is $m^*_{\rm D\,s} \equiv m_{\rm N} - g_{\sigma{\rm N}}\sigma = 0.7m_{\rm N}$, where $m_{\rm N} \equiv (m_{\rm n} + m_{\rm p})/2 \approx 938.919$ MeV. The model is then extended to the NH matter. The vector-meson coupling constants with hyperons are obtained from the nucleon ones using the SU(6) symmetry. The scalar σ^* meson is not included. Inclusion of the vector ϕ meson producing repulsion between hyperons is sufficient to make the model (marginally) consistent with 2.0 $M_\odot$ pulsars.

GM1′B. The saturation baryon number density is the same as for **GM1A**, $n_{\rm s} = 0.153$ fm^{-3}. The nuclear matter incompressibility at saturation point, $K_{\rm s} = 240$ MeV, is within typical semi-empirical evaluations of $K_{\rm s}$: it is significantly lower than that obtained for the **GM1A** model. In contrast, the symmetry energy and the Dirac effective nucleon mass are the same as those obtained for the **GM1A** model. In the NH matter, the vector ϕ meson is included, while the scalar σ^* is not present. In spite of a significantly lower $K_{\rm s}$, compared to that obtained for **GM1A**, the value of $M_{\rm max}$ is above 2.0 $M_\odot$. This is due to a breaking of the SU(6) symmetry in the vector-meson couplings to hyperons. Using notation of Weissenborn et al. (2012b), this symmetry breaking is characterized by $z = 0.3$, which is significantly smaller than $z = 1/\sqrt{6} \simeq 0.408$ corresponding to the SU(6)-symmetric case.

TM1C. It reduces to the widely used **TM1** model in the nucleon sector, see Sugahara & Toki (1994). For the latter model $n_{\rm s} = 0.145$ fm^{-3}. The nuclear matter incompressibility, $K_{\rm s} = 281$ MeV is on the high-side of semi-empirical evaluations. The Dirac effective nucleon mass in symmetric nuclear matter at saturation point is rather small, $m^*_{\rm D\,s} = 0.634m_{\rm N}$, where $m_{\rm N}$ is chosen to be $m_{\rm N} \equiv 938$ MeV for this model. The nuclear symmetry energy, $E_{\rm sym} = 36.9$ MeV, is higher than typical semi-empirical evaluations. Extension of **TM1** to NH matter includes the vector ϕ meson *and* the scalar σ^* meson. The breaking of the SU(6) symmetry is even stronger than for the **GM1′B** model, and corresponds to $z = 0.2$. In addition to fitting the $U_\Lambda^{\rm (N)}$, $U_\Xi^{\rm (N)}$, and $U_\Sigma^{\rm (N)}$ potential well depths, this model also fits a weak $\Lambda-\Lambda$ attraction, $U_\Lambda^{(\Lambda)} = -5.0$ MeV (Takahashi et al. 2001), and assumes $U_\Xi^{(\Xi)} \approx U_\Lambda^{(\Xi)} \approx 2U_\Xi^{(\Lambda)} \approx 2U_\Lambda^{(\Lambda)} \approx -10.0$ MeV (Schaffner et al. 1994). Maximum allowable mass is 2.056 $M_\odot$.

The EOSs for these models, $P = P(\rho)$, are plotted in Fig. 1. The way they are obtained is briefly discussed in Appendix B. One notices that for $\rho \gtrsim 2\times10^{15}$ g cm^{-3} the EOS **TM1C** is the softest one. And still, it yields the highest value of $M_{\rm max}$. This apparent paradox can be explained as follows. $M_{\rm max}$ is a functional of the EOS, $M_{\rm max}[P(\rho < \rho_{\rm max})]$, but the EOS for ρ greater than the maximum central density in *stable* NSs does not affect the value of $M_{\rm max}$. **TM1C** is actually the stiffest for $\rho \lesssim 1.4\times10^{15}$ g cm^{-3}, which is quite close to the maximum central density $\rho_{\rm max} \approx 1.85\times10^{15}$ g cm^{-3} for stable NS based on this EOS. Therefore, while **TM1C** is the softest EOS for $\rho \gtrsim 2\times10^{15}$ g cm^{-3}, this is irrelevant for the value of $M_{\rm max}$.

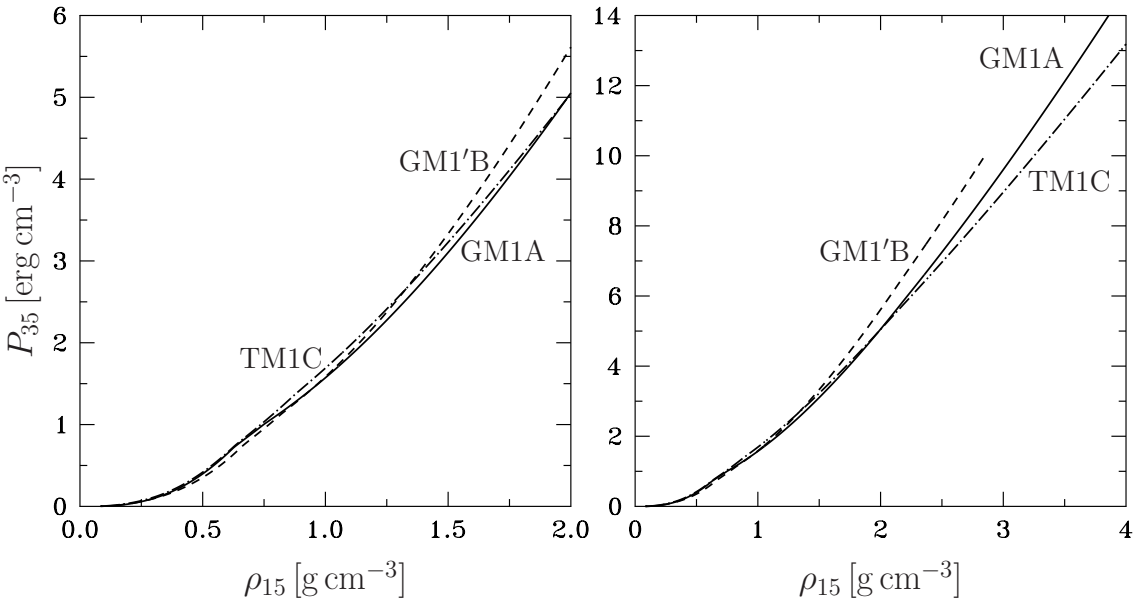

Figure 1. Pressure $P_{35} = P/10^{35}$ versus density $\rho_{15} = \rho/10^{15}$ for three models of NH matter considered in this paper. *Right-hand panel:* Overall plots of EOSs. For $\rho_{15} > 2$, the **TM1C** EOS is the softest, and **GM1′B** the stiffest. *Left-hand panel:* Lower-density, $\rho_{15} < 2$, segments of the EOSs. The ordering of the EOSs according to their stiffness depends on the density interval. For further discussion of this effect and its impact on the value of $M_{\max}$ see the text.

Model	$n_{\rm b}^{(\mu)}$ ($\mathrm{fm^{-3}}$)	$n_{\rm b}^{(\Lambda)}$ ($\mathrm{fm^{-3}}$)	$n_{\rm b}^{(\Xi^-)}$ ($\mathrm{fm^{-3}}$)	$n_{\rm b}^{(\Xi^0)}$ ($\mathrm{fm^{-3}}$)	$n_{\rm b,max}$ ($\mathrm{fm^{-3}}$)
GM1A	0.1271	0.3472	0.4076	–	0.923
GM1′B	0.1272	0.3669	0.4438	0.9750	1.018
TM1C	0.1090	0.3466	0.4622	–	0.856

Table 2. Thresholds $n_{\rm b}^{(k)}$ of appearance of particles $k = \mu$, Λ, Ξ^-, and Ξ^0 for which $n_{\rm b}^{(k)} < n_{\rm b,max}$ (see the last column). Only model **GM1′B** admits the existence of Ξ^0 hyperons in stable NSs.

6.2 Particle fractions, adiabatic indices, and the speed of sound

In Fig. 2 we show the particle fractions of constituents of NH matter, $y_i \equiv n_i/n_{\rm b}$, as functions of baryon number density $n_{\rm b}$. Three panels correspond to three RMF models (**GM1A**, **GM1′B**, and **TM1C**). Dot-dashed vertical lines correspond to the maximum baryon number density reachable in stable non-rotating NSs, see Table 1. The order of appearance of hyperons with increasing density is identical for all EOSs. The corresponding thresholds are presented in Table 2. The first hyperon to appear is Λ, the second hyperon is Ξ^-. The third hyperon, Ξ^0, appears only in model **GM1′B** and exists only in configurations close to the $M_{\max}$ one, thus playing a marginal role in stable stars. A large repulsive potential energy of Σ^- in nuclear matter makes its threshold density very high, from $9n_0$ for **TM1C** to more than $10n_0$ for **GM1A**. Therefore, Σ^- are absent in stable NSs.

An important quantity characterizing dynamic properties of stellar matter is the adiabatic index

$$\gamma = \frac{P+\rho}{P}\,\frac{\delta P}{\delta \rho}, \tag{69}$$

where δP is a small deviation of the pressure P from its equilibrium value caused by a small variation $\delta\rho$ of the energy density ρ. This index is related to the speed of sound s by the equality $s = [\gamma P/(P+\rho)]^{1/2}$. The ratio $\delta P/\delta\rho$ in Eq. (69) should be calculated under a number of additional conditions (such as quasineutrality, chemical equilibrium etc.), which differ depending on a timescale τ of a physical process under consideration [1]. The resulting adiabatic indices γ will also be different.

Here we consider three adiabatic indices: equilibrium adiabatic index $\gamma_{\rm eq}$ (Haensel, Potekhin & Yakovlev 2007), frozen adiabatic index $\gamma_{\rm fr}$ (Haensel et al. 2007), and 'partly frozen' adiabatic index $\gamma_{\rm part\,fr}$. In Fig. 3 they are shown by, respectively, dot-dashed, solid, and dashed lines as functions of $n_{\rm b}$ for the three models of NH matter adopted in this paper.

[1] The most natural example of such process is the NS oscillations. Then $\tau \sim 1/\omega$, where ω is the oscillation frequency.

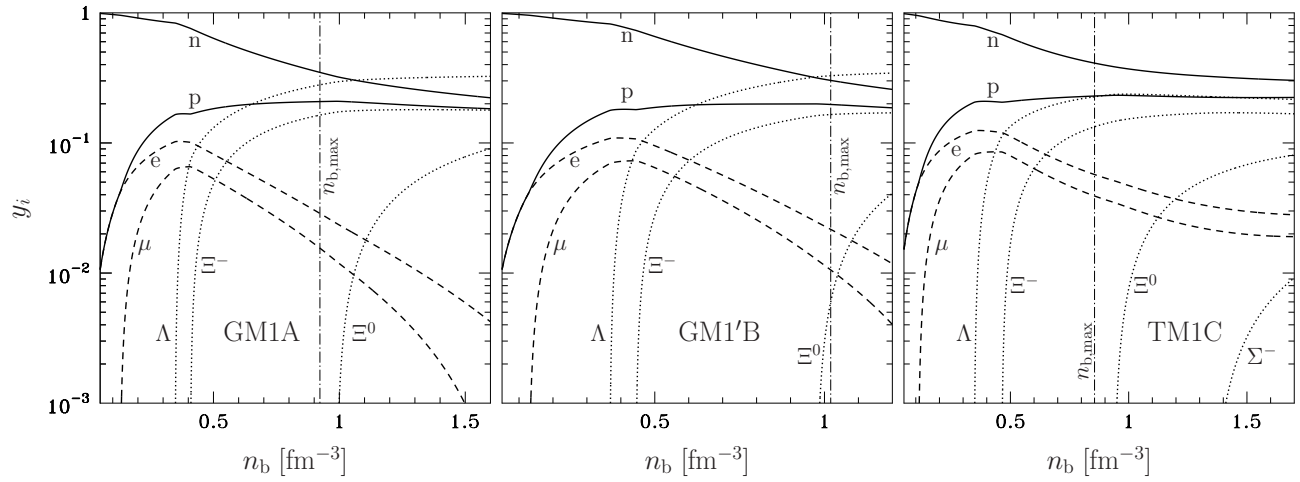

Figure 2. Particle fractions $y_i = n_i/n_{\rm b}$ versus baryon number density $n_{\rm b}$ for three EOSs, **GM1A**, **GM1′B**, and **TM1C**. The vertical dot-dashed lines correspond to the maximum baryon number density reached in stable non-rotating NSs for a given EOS, see Table 1. For further details see Sect. 6.2.

The index $\gamma_{\rm eq}$ naturally appears in the situation when the dynamical process of interest is very slow. This means that $\tau \gg \tau_{\rm strong}$ and $\tau \gg \tau_{\rm weak}$, where $\tau_{\rm strong}$ and $\tau_{\rm weak}$ are the characteristic timescales of 'fast' (due to strong interaction) and 'slow' (due to weak interaction) reactions of particle mutual transformations, which move the system towards full thermodynamic equilibrium (see, e.g., Yakovlev et al. 2001; Kantor & Gusakov 2009).

The index $\gamma_{\rm fr}$ can be introduced (e.g., Haensel et al. 2007) in the opposite limit, when $\tau \ll \tau_{\rm strong}$ and $\tau \ll \tau_{\rm weak}$. In that case the process is so fast that *all* the reactions are effectively 'frozen' on a dynamical timescale τ. Mathematically, this means that the particle fractions y_i remain constant during this process for *any* particle species i = e, μ, n, p, Λ, ...: $y_i = n_i/n_{\rm b} =$ constant.

Finally, the index $\gamma_{\rm part\,fr}$ is introduced in the intermediate case, when $\tau_{\rm weak} \gg \tau \gg \tau_{\rm strong}$. In that case the matter is in equilibrium with respect to the fast reactions, while slow reactions (such as, e.g., Urca reactions; see Haensel et al. 2007) are frozen. In stable NSs the fast reactions are: $\mathrm{p} + \Xi^- \leftrightarrow \Lambda + \Lambda$ and $\mathrm{n} + \Xi^0 \leftrightarrow \Lambda + \Lambda$. The adiabatic indices are considered in more detail in Appendix C.

As follows from Fig. 3, each time, when a hyperon species appears as $n_{\rm b}$ increases, we see a sharp drop of the equilibrium adiabatic index $\gamma_{\rm eq}$. Such drops reflect the fact that appearance of hyperons makes the EOS softer. The magnitude of the hyperon-threshold drops decreases with increasing density, with the largest drop at the threshold for Λ's. This is not surprising and is related to the increasing number of baryon species with growing density (the more the baryon species, the less sensitive is $\gamma_{\rm eq}$ to the appearance of additional hyperon species).

In contrast to $\gamma_{\rm eq}$, $\gamma_{\rm fr}$ (and $\gamma_{\rm part\,fr}$, which is practically indistinguishable from $\gamma_{\rm fr}$) does not drop sharply near the hyperon thresholds: The influence of hyperon thresholds is less pronounced if we consider rapid processes with $\tau \ll \tau_{\rm strong}$ and $\tau \ll \tau_{\rm weak}$.

For illustration, Fig. 4 shows the equilibrium speed of sound $s_{\rm eq} = [\gamma_{\rm eq} P/(P+\rho)]^{1/2}$ for the three EOSs considered in this paper.

6.3 Effective masses

Our results for normalized Landau effective masses $\overline{m}_i^* \equiv m_i^*/m_i$ [see Eq. (30)] are shown in Fig. 5.

For all EOSs at all densities $\overline{m}_{\rm n}^* > \overline{m}_{\rm p}^*$, and, moreover, at densities relevant to stable NSs $\overline{m}_{\Xi^-}^* > \overline{m}_{\Xi^0}^* > \overline{m}_{\Lambda}^* > \overline{m}_{\rm n}^* > \overline{m}_{\rm p}^*$. At the same time one notices a systematic differences in $\overline{m}_{i_{\rm H}}^*(n_{\rm b})$ curves (hereafter $i_{\rm H} = \Lambda, \Xi^-, \Xi^0, \Sigma^-$) between three dense matter models used.

For **GM1A** all hyperon $\overline{m}_{i_{\rm H}}^*$ curves are very flat, ranging from 0.7 to 0.85. For **GM1′B** model, the values of $\overline{m}_{i_{\rm H}}^*$ are systematically smaller, about $0.6 - 0.75$. The strongest Fermi-liquid effect and density dependence are obtained for **TM1C** model, $\overline{m}_{i_{\rm H}}^*$ fall into the range $0.5 - 0.65$.

We conclude that there is a significant model dependence of $\overline{m}_i^*(n_{\rm b})$ for hyperons. This fact reflects limitations of our knowledge of the N–H and H–H interactions in dense NH matter.

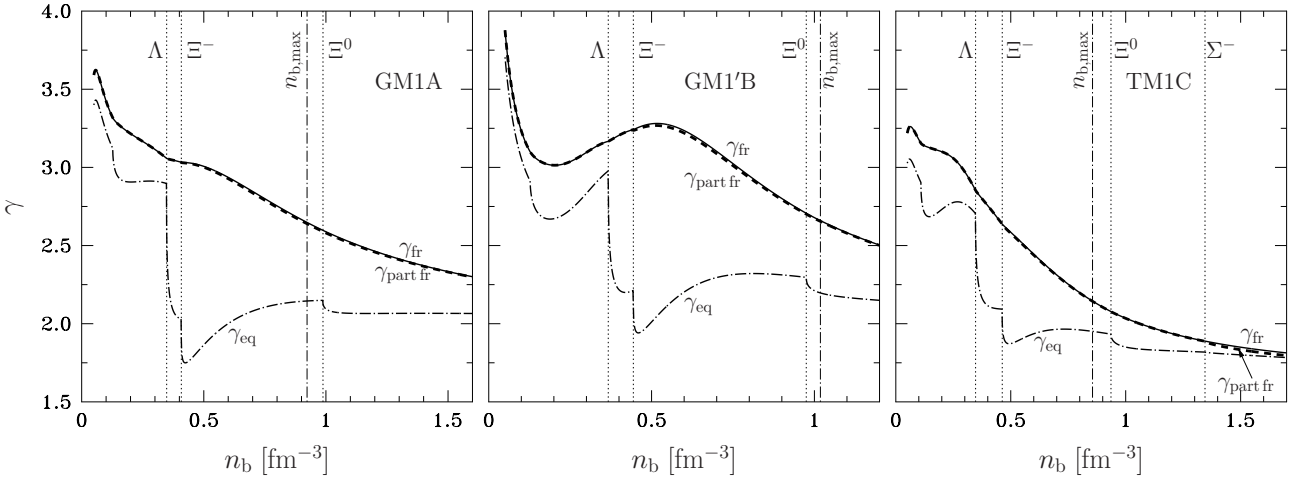

Figure 3. Three adiabatic indices versus $n_{\rm b}$ for the three selected models of NH matter. $\gamma_{\rm eq}$ (dot-dashed lines) is calculated assuming full thermodynamic equilibrium; $\gamma_{\rm fr}$ (solid lines) is obtained under assumption that all reactions of particle mutual transformations are frozen (completely frozen matter composition); $\gamma_{\rm part\ fr}$ (dashed lines) assumes equilibrium with respect to the 'fast' reactions, while 'slow' reactions are frozen (see Sect. 6.2 for details). Vertical dotted lines indicate thresholds of appearance of (from left to right) Λ, Ξ^-, Ξ^0, and Σ^- hyperons. Vertical dot-dashed lines show the maximum baryon number density in a non-rotating NS of a maximum allowable mass (see also Table 1).

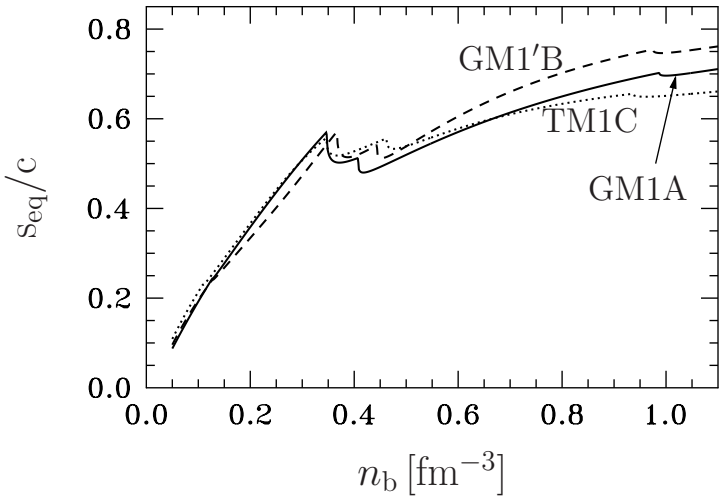

Figure 4. Equilibrium sound speed $s_{\rm eq} = [\gamma_{\rm eq} P/(P+\rho)]^{1/2}$ (in units of speed of light c) versus $n_{\rm b}$ for three models of NH matter.

6.4 Landau Fermi-liquid parameters f_0^{ij}, f_1^{ij}, and entrainment matrix Y_{ij}

Our results for dimensionless Landau Fermi-liquid parameters $F_0^{ij} = F_0^{ji}$ and $F_1^{ij} = F_1^{ji}$ are collected in Figs. 6 and 7, respectively. The results for normalized dimensionless entrainment matrix $Y_{ij} = Y_{ji}$ are shown in Fig. 8.

Landau parameters $F_0^{i_{\rm N} j_{\rm N}}$ (hereafter $i_{\rm N} = {\rm n}, {\rm p}$) for **GM**-type models have similar values and density dependence, those for **TM1C** model are smaller and are more similar to Gusakov et al. (2009b) results. In contrast to Gusakov et al. (2009b), Landau parameters $F_0^{i_{\rm H} j_{\rm H}}$ are all positive except for $F_0^{{\rm p}\Sigma^-}$ in the model **TM1C** and $F_0^{{\rm p}\Xi^-}$ in the model **GM1A** near the threshold for the Ξ^- hyperon.

Nucleon $\ell = 1$ Landau parameters $F_1^{i_{\rm N} j_{\rm N}}$ are not so much model sensitive, they are quite similar for the three models developed here and also for the model of Gusakov et al. (2009b). We find that, as a rule, the $\ell = 1$ Landau parameters are negative. A few ones which are positive, remain very small. $F_1^{\rm nn}$ dominates in magnitude over remaining Landau parameters, but $F_1^{\rm pp}$ becomes comparable to it at the largest densities. Model dependence of Landau parameters with $i_{\rm N} j_{\rm H}$ and $i_{\rm H} j_{\rm H}$ indices is more significant.

The entrainment matrix elements Y_{ij} are also not very model dependent. The bundle of $Y_{i j_{\rm H}}$ is bound by $Y_{\Lambda\Lambda}$ from above and by (negative) $Y_{{\rm n}\Lambda}$ from below. $Y_{\Xi^-\Xi^-}$ is significantly smaller than $Y_{\Lambda\Lambda}$. Non-diagonal matrix elements Y_{ij} with $i \neq j$ are

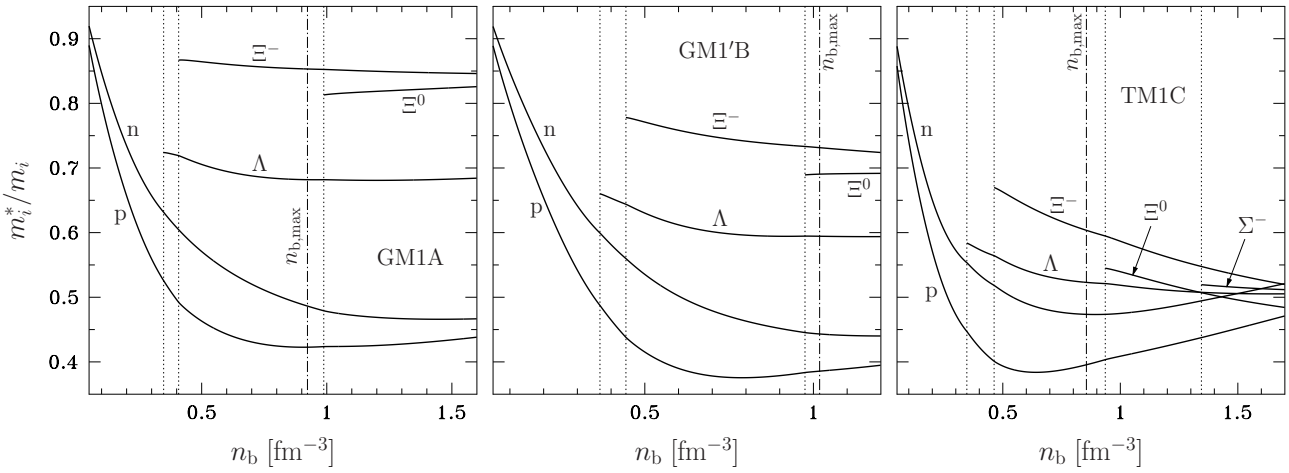

Figure 5. The normalized Landau effective masses m_i^*/m_i versus $n_{\rm b}$ for three EOSs. Each curve is marked by a corresponding baryon species index $i =$ n, p, Λ, ... Other notations are the same as in Fig. 3.

significantly smaller than Y_{ii} or Y_{jj}, and are usually negative; if positive, they are close to zero. On the opposite, diagonal elements Y_{ii} are positive.

6.5 Stability with respect to $\ell = 0$ and $\ell = 1$ deformations of the Fermi surfaces

A small $\ell = 0$ deformation of the i-Fermi surface induces a small perturbation δn_i of particle number density n_i, and vice versa. We consider only long-wave (uniform) perturbations that preserve electric charge neutrality of the system (in order to exclude the stabilizing effect of the Coulomb energy; see Gusakov et al. 2009b for details). Then the stability requirement is equivalent to the positive definiteness of the quadratic form $\sum_{km} A_{km}\delta n_k \delta n_m$, where the indices k and m run over all particle species, except for electrons. The matrix A_{km} is expressible in terms of the Fermi-liquid parameters F_0^{ij} (see, e.g., Gusakov et al. 2009b, and references therein). Stability with respect to perturbation δn_i imposes a number of conditions on F_0^{ij}. We checked that these stability conditions are satisfied within the liquid NS core, i.e., for $n_{\rm b} > 0.1$ fm^{-3}, for all considered models.

A small $\ell = 1$ deformation of the i-superfluid Fermi surface keeps the value of n_i unchanged but induces a uniform superfluid current associated with $\boldsymbol{Q}_i$. The change of the energy density associated with superfluid currents is given by a quadratic form $\frac{1}{2}\sum_{ij} Y_{ij}\boldsymbol{Q}_i\boldsymbol{Q}_j$, see Gusakov et al. (2009b). Stability of the ground state is equivalent to the positive definiteness of the matrix Y_{ij}, implying a number of conditions on the parameters F_1^{ij}. We checked that these conditions are satisfied for all the three models and at all densities relevant to NSs.

Recently, Gulminelli, Raduta & Oertel (2012) and Gulminelli et al. (2013) pointed out the first-order phase transition associated with the appearance of strangeness in dense baryonic matter. This first-order phase transition is signalled by a spinodal instability of an uniform baryon matter (nΛ-matter in Gulminelli et al. 2012, npΛe-matter in Gulminelli et al. 2013). In our calculations, the matrix A_{ij} of Sect. 6.5 is positive definite at $n_{\rm b} > 0.1$ fm^{-3} and appearance of Λ is continuous (second-order phase transition): we do not find spinodal instability associated with appearance of strangeness that would indicate a phase-separation instability. However, in contrast to Gulminelli et al. (2012, 2013) we consider exclusively baryon matter with no trapped neutrinos and close to beta equilibrium. Therefore, our particle fractions y_i *in equilibrium* result from the weak interaction equilibrium conditions (see Eq. B1), and are functions of $n_{\rm b}$, $y_j = y_j^{(\rm eq)}(n_{\rm b})$. Our trajectory $y_j = y_j^{(\rm eq)}(n_{\rm b})$ does not cross a spinodal instability region.

7 SUMMARY OF RESULTS

We develop a general scheme for calculation of the $\ell = 0, 1$ Landau Fermi-liquid parameters, valid for a broad class of nonlinear RMF models of dense baryon matter. A nonlinear Lagrangian that we consider involves the octet of baryons coupled to the $\sigma\omega\rho\phi\sigma^*$ mesons. It includes quartic terms in meson fields.

Knowledge of the Landau Fermi-liquid parameters is crucial for modelling NSs because it allows one to directly calculate the following important quantities: (*i*) the thermodynamic derivatives $\partial\mu_i/\partial n_j$ [see Eqs. (68) and (D1)], where μ_i and n_j are the relativistic chemical potential and the number density of particle species i and j, respectively; (*ii*) the relativistic entrainment matrix Y_{ij}, both at zero temperature [see Eq. (12)] and at finite temperatures (see Gusakov et al. 2009a); this is a basic parameter for superfluid NSs.

The developed general scheme has been applied to study in detail three up-to-date specific RMF models of NH matter,

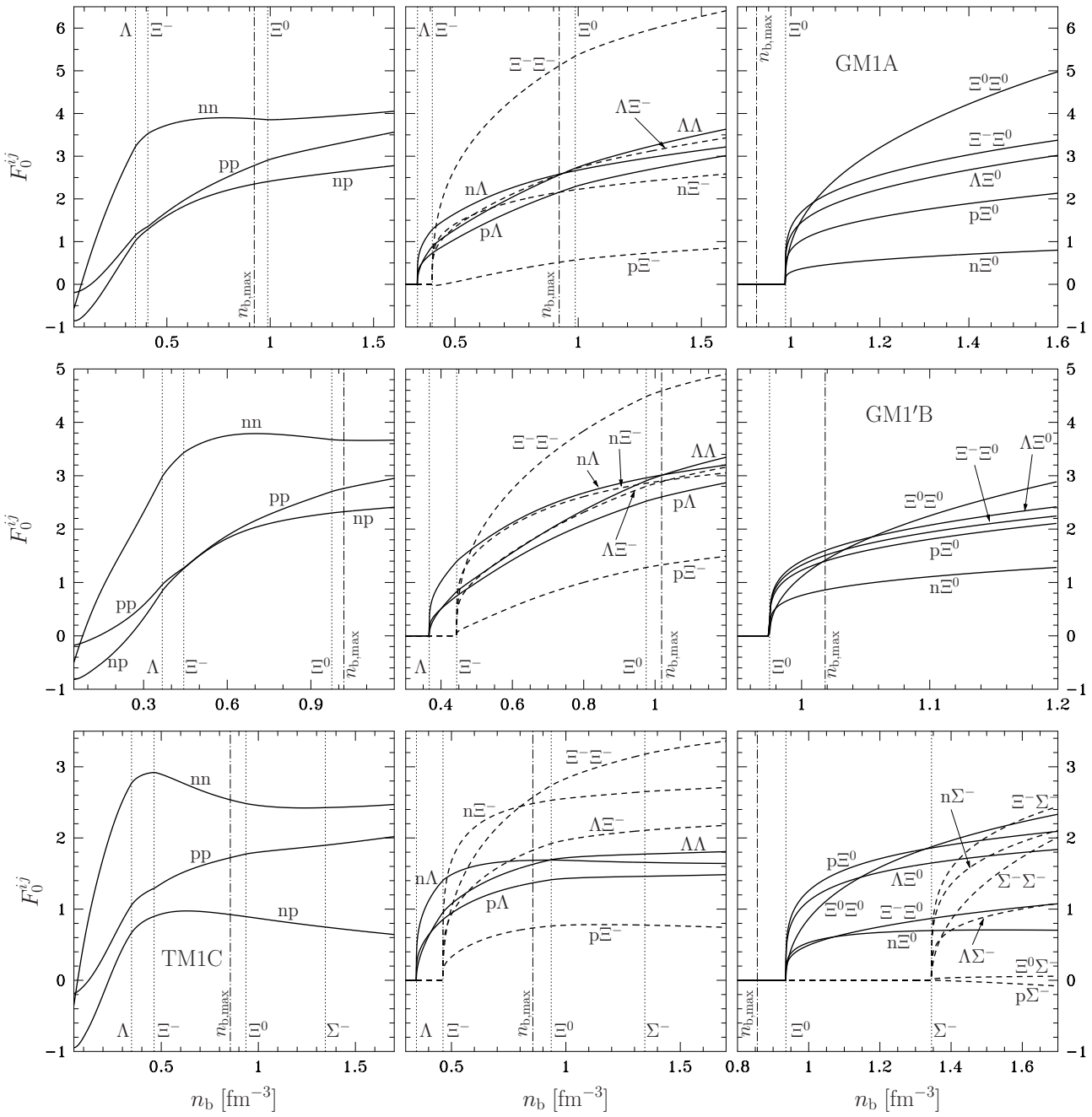

Figure 6. The dimensionless Landau Fermi-liquid parameters F_0^{ij} versus baryon number density for **GM1A** (upper panels), **GM1′B** (middle panels), and **TM1C** (bottom panels) RMF models. Each curve is marked by the corresponding symbol ij. Other notations are the same as in Fig. 3.

which are consistent with the existence of 2 $M_\odot$ pulsars (PSR J1614-2230 and J0348+0432; see Demorest et al. 2010; Antoniadis et al. 2013) and with semi-empirical nuclear and hypernuclear data.

These models allow for the presence of (maximum) three hyperon species in stable NSs. Two of the models (**GM1A** and **GM1′B**) predict the appearance of (with increasing density) Λ and Ξ^- hyperons, while the model **TM1C** predicts also appearance of Ξ^0 hyperons close to a maximum density reachable in stable NSs for this model. It is interesting that, in contrast to, e.g., the paper by Gusakov et al. (2009b), Σ^- hyperons do not appear in stable NSs for the selected RMF models because of their large repulsive potential energy in nuclear matter.

For all models we calculated and analysed the Landau Fermi-liquid parameters F_0^{ij} and F_1^{ij} as functions of the baryon number density $n_{\rm b}$, entrainment matrix $Y_{ij}(n_{\rm b})$ at $T = 0$, EOS [pressure versus density relation $P(\rho)$], particle number densities $n_i(n_{\rm b})$, adiabatic indices, and Landau effective masses.

All obtained numerical results for the three RMF models constructed by us are available on-line as a public domain at:

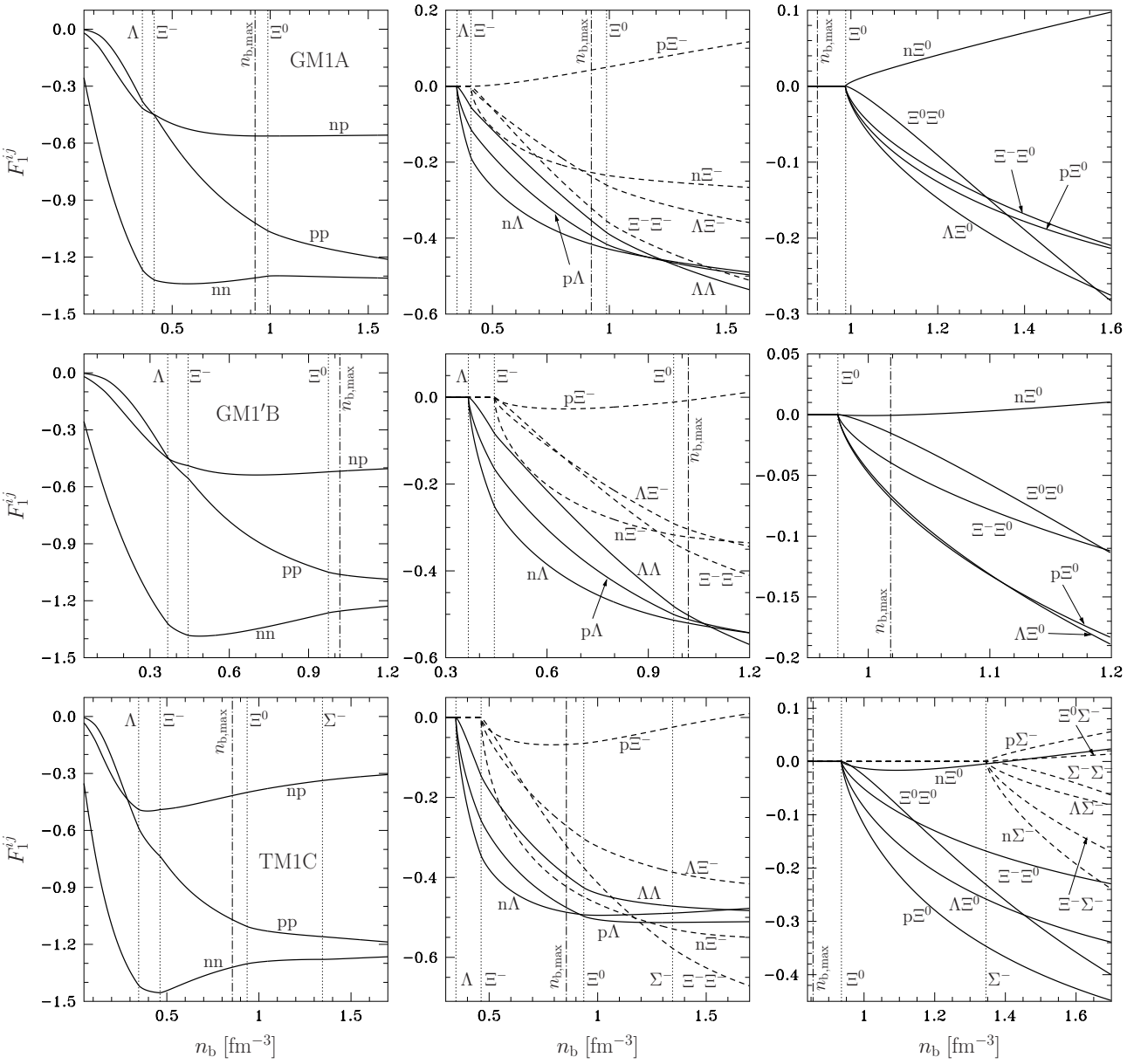

Figure 7. The same as Fig. 6, but for F_1^{ij}.

http://www.ioffe.ru/astro/NSG/heos/hyp.html. This data source contains all necessary information to model dynamics of superfluid NSs, e.g., their oscillations and cooling. The description of the on-line material is presented in the Appendix D.

ACKNOWLEDGEMENTS

This work was partially supported by RF president programme (grants MK-857.2012.2 and NSh-4035.2012.2), by RFBR (grants 11-02-00253-a and 12-02-31270-mol-a), by the Ministry of Education and Science of Russian Federation (agreement no. 8409, 2012), and by the Polish NCN research grant no. 2011/01/B/ST9/04838.

REFERENCES

Andersson N., Baker J., Belczynski K., Bernuzzi S., Berti E., et al. 2013, ArXiv e-prints

Andersson N., Ferrari V., Jones D. I., Kokkotas K. D., Krishnan B., Read J. S., Rezzolla L., Zink B., 2011, Gen. Rel. Grav. 43, 409

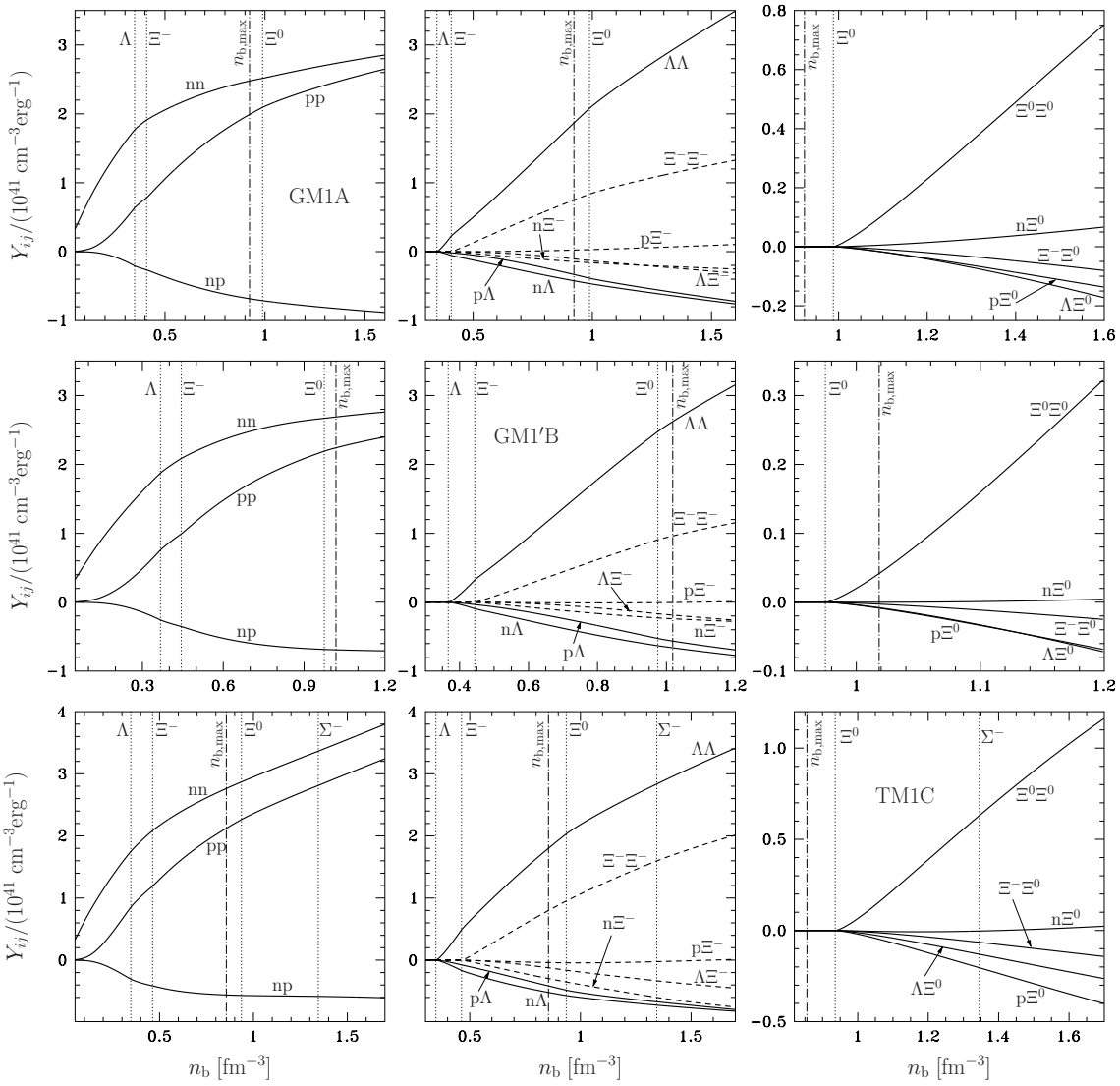

Figure 8. The same as Fig. 6, but for normalized elements of symmetric matrix Y_{ij}. For readability of the figure, we do not plot bunch of curves corresponding to the elements $Y_{i\Sigma^-}$ of the entrainment matrix.

Antoniadis J., Freire P. C. C., Wex N., Tauris T. M., Lynch R. S., et al. 2013, Science, 340, 448

Baym G., Chin S. A., 1976, Nucl. Phys. A, 262, 527

Baym G., Pethick C., 1991, Landau Fermi-liquid theory: concepts and applications (Wiley-VCH, Weinheim)

Bednarek I., Haensel P., Zdunik J. L., Bejger M., Mańka R., 2012, A&A, 543, A157

Bednarek I., Manka R., 2009, Journal of Physics G Nuclear Physics, 36, 095201

Demorest P. B., Pennucci T., Ransom S. M., Roberts M. S. E., Hessels J. W. T., 2010, Nature, 467, 1081

Glendenning N., 2000, Compact stars (Astronomy and Astrophysics Library, Springer-Verlag, New York)

Glendenning N. K., 1985, ApJ, 293, 470

Glendenning N. K., Moszkowski S. A., 1991, Phys. Rev. Lett. , 67, 2414

Gulminelli F., Raduta A. R., Oertel M., 2012, Phys. Rev. C, 86, 025805

Gulminelli F., Raduta A. R., Oertel M., Margueron J., 2013, Phys. Rev. C, 87, 055809

Gusakov M. E., 2007, Phys. Rev. D, 76, 083001

Gusakov M. E., Kantor E. M., 2008, Phys. Rev. D, 78, 083006

Gusakov M. E., Kantor E. M., Haensel P., 2009a, Phys. Rev. C, 80, 015803

Gusakov M. E., Kantor E. M., Haensel P., 2009b, Phys. Rev. C, 79, 055806

Haensel P., Potekhin A. Y., Yakovlev D. G., 2007, Neutron Stars 1 : Equation of State and Structure (Astrophysics and Space Science Library, Springer, New York)

Kantor E. M., Gusakov M. E., 2009, Phys. Rev. D, 79, 043004

Leggett A. J., 1965, Phys. Rev. , 140, 1869
Leggett A. J., 1975, Rev. Mod. Phys. , 47, 331
Millener D. J., Dover C. B., Gal A., 1988, Phys. Rev. C, 38, 2700
Pines D., Nozieres P., 1999, Theory of quantum liquids (Westview Press, Boulder)
Schaffner J., Dover C. B., Gal A., Greiner C., Millener D. J., Stocker H., 1994, Annals of Physics, 235, 35
Schaffner-Bielich J., Gal A., 2000, Phys. Rev. C, 62, 034311
Shen H., Yang F., Toki H., 2006, Prog. Theor. Phys. 115, 325
Sugahara Y., Toki H., 1994, Nucl. Phys. A, 579, 557
Takahashi H., Ahn J. K., Akikawa H., Aoki S., Arai K., et al. 2001, Phys. Rev. Lett. , 87, 212502
Weissenborn S., Chatterjee D., Schaffner-Bielich J., 2012a, Nucl. Phys. A, 881, 62
Weissenborn S., Chatterjee D., Schaffner-Bielich J., 2012b, Phys. Rev. C, 85, 065802
Yakovlev D. G., Kaminker A. D., Gnedin O. Y., Haensel P., 2001, Phys. Rep. , 354, 1
Yang F., Shen H., 2008, Phys. Rev. C, 77, 025801

APPENDIX A: COUPLING CONSTANTS

Here we discuss the coupling constants for models **GM1A**, **GM1′B**, and **TM1C**. The main parameters characterizing these models are summarized in Table A1. The actual values of hyperon and meson masses which were used in all calculations are presented in Table A2 (note that the masses of baryons in each isomultiplet are assumed to be the same). For all the models $\Lambda_{\rm V} = \widetilde{c}_3 = 0$. The data which are not included in Table A1 are the depths of potential wells for hyperons in symmetric nuclear matter at saturation density (e.g., Millener et al. 1988; Schaffner-Bielich & Gal 2000; Shen, Yang & Toki 2006; Weissenborn et al. 2012a),

$$U_\Lambda^{(\rm N)} = -28.0 \text{ MeV}, \quad U_\Xi^{(\rm N)} = -18.0 \text{ MeV}, \quad U_\Sigma^{(\rm N)} = 30.0 \text{ MeV}, \tag{A1}$$

which are the same for all three models. In addition, the model **TM1C**, which allows for the presence of σ^* meson, fits also the weak $\Lambda - \Lambda$ attraction (Takahashi et al. 2001),

$$U_\Lambda^{(\Lambda)} = -5.0 \text{ MeV}, \tag{A2}$$

and assumes (Schaffner et al. 1994)

$$U_\Xi^{(\Xi)} \approx U_\Lambda^{(\Xi)} \approx 2U_\Xi^{(\Lambda)} \approx 2U_\Lambda^{(\Lambda)} = -10.0 \text{ MeV}. \tag{A3}$$

Using these data, one can calculate various coupling constants for the models **GM1A**, **GM1′B**, and **TM1C**. Most of them are listed in Table A3. The remaining constants are related to these from Table A3 by the following conditions (see, e.g., equation (11) of Weissenborn et al. 2012b)

$$g_{\omega\Lambda} = \frac{\sqrt{2}}{\sqrt{2}+\sqrt{3}z}\, g_{\omega\rm N}, \;\; g_{\omega\Sigma} = g_{\omega\Lambda}, \;\; g_{\omega\Xi} = \frac{\sqrt{2}-\sqrt{3}\,z}{\sqrt{2}+\sqrt{3}\,z}\, g_{\omega\rm N}, \tag{A4}$$

$$g_{\rho\Lambda} = 0, \;\; g_{\rho\Sigma} = g_{\rho\rm N}, \;\; g_{\rho\Xi} = g_{\rho\rm N}, \tag{A5}$$

$$g_{\phi\rm N} = \frac{\sqrt{6}\,z-1}{\sqrt{2}+\sqrt{3}\,z}\, g_{\omega\rm N}, \;\; g_{\phi\Lambda} = g_{\phi\Sigma} = -\frac{1}{\sqrt{2}+\sqrt{3}\,z}\, g_{\omega\rm N}, \;\; g_{\phi\Xi} = -\frac{1+\sqrt{6}\,z}{\sqrt{2}+\sqrt{3}\,z}\, g_{\omega\rm N}. \tag{A6}$$

Let us briefly describe how we calculated the coupling constants presented in Table A3. The constants g_3, g_4, $g_{\sigma\rm N}$, $g_{\omega\rm N}$, and $g_{\rho\rm N}$ can be expressed through the parameters $n_{\rm s}$, $B_{\rm s}$, $E_{\rm sym}$, $K_{\rm s}$, and $m^*_{\rm D\,s}$. The corresponding consideration is similar to that presented in section 4.8 of Glendenning (2000) with the only exception that in our case ϕ can be non-vanishing even for pure nucleon matter [because $g_{\phi\rm N}$ is nonzero and is related to $g_{\omega\rm N}$ by Eq. (A6)].

The constants $g_{\sigma i}$, where $i = \Lambda$, Σ, and Ξ, can be obtained from the requirement that the energy of an i-hyperon (with the momentum $\boldsymbol{p} = 0$) in the symmetric nuclear matter *at saturation* is equal to $U_i^{(\rm N)}$, that is

$$m_i + U_i^{(\rm N)} = g_{\omega i}\omega^0 + g_{\phi i}\phi^0 + (m_i - g_{\sigma i}\sigma). \tag{A7}$$

To use this formula one should first calculate the fields σ, ω^0, and ϕ^0 using, respectively, Eqs. (20), (22), and (24). Note that nucleons do not generate the σ^*-field, and $\rho^0_3 = 0$ in symmetric nuclear matter.

Finally, following Yang & Shen (2008), the constants $g_{\sigma^* i}$ ($i = \Lambda$, Ξ) for the model **TM1C** are calculated assuming $U_i^{(\Xi)} = -10$ MeV [see Eq. (A3)]. To calculate them we consider symmetric matter at $n = n_{\rm s}$ composed of equal number of Ξ^- and Ξ^0 hyperons, and add one more i-hyperon with momentum $\boldsymbol{p} = 0$ to this system. Then the energy of this i-hyperon will be

$$m_i + U_i^{(\Xi)} = g_{\omega i}\omega^0 + g_{\phi i}\phi^0 + (m_i - g_{\sigma i}\sigma - g_{\sigma^* i}\sigma^*), \tag{A8}$$

so that $g_{\sigma^* i}$ can be easily found from this formula provided that the fields σ, σ^*, ω^0, ϕ^0 are already calculated from Eqs.

Model	$m_{\rm N}$ (MeV)	$n_{\rm s}$ (fm^{-3})	$B_{\rm s}$ (MeV)	$E_{\rm sym}$ (MeV)	$K_{\rm s}$ (MeV)	$m^*_{\rm D\,s}/m_{\rm N}$	c_3	z	σ^*
GM1A	938.919	0.153	-16.3	32.5	300.0	0.7	0.0	$1/\sqrt{6}$	No
GM1′B	938.919	0.153	-16.3	32.5	240.0	0.7	0.0	0.3	No
TM1C	938.0	0.145	-16.3	36.9	281.0	0.634	71.3075	0.2	Yes

Table A1. Various physical parameters for three models: **GM1A**, **GM1′B**, and **TM1C**. In the table $m_{\rm N}$ is the nucleon mass; $n_{\rm s}$ the saturation density; $B_{\rm s}$ binding energy per nucleon; $E_{\rm sym}$ the symmetry energy; $K_{\rm s}$ nuclear matter incompressibility and $m^*_{\rm D\,s}/m_{\rm N}$ the Dirac effective mass in units of $m_{\rm N}$. All these quantities are given at saturation point. Further, c_3 is the coupling constant characterizing non-linear interaction of ω-mesons; z is the parameter introduced in Weissenborn et al. 2012b to describe deviation of a given model from the SU(6)-symmetric case (the SU(6) value is $z = 1/\sqrt{6}$). Finally, the last column indicates that σ^*-mesons are only allowed for **TM1C** model.

Mass,	m_Λ	m_Σ	m_Ξ	m_σ	m_ω	m_ρ	m_ϕ	m_{σ^*}
MeV	1115.63	1193.12	1318.1	511.198	783.0	770.0	1020.0	975.0

Table A2. Masses (in MeV) of hyperons and mesons adopted in all calculations.

(20)–(22) and (24). Note that $\rho^0_3 = 0$ in symmetric matter is composed of Ξ^- and Ξ^0 hyperons. The constant $g_{\sigma^*\Sigma}$ is set equal to $g_{\sigma^*\Lambda}$.

APPENDIX B: EQUATION OF STATE

Here we consider beta-equilibrated NH matter. The condition of beta-equilibrium implies the following relations between the relativistic chemical potentials (e.g., Haensel et al. 2007),

$$\mu_i = \mu_{\rm n} - q_i\mu_{\rm e}, \quad \mu_{\rm e} = \mu_\mu, \tag{B1}$$

where q_i is the charge of baryon species i in units of the proton charge. These equations should be supplemented by the quasineutrality condition,

$$\sum_i q_i n_i - n_{\rm e} - n_\mu = 0. \tag{B2}$$

Together with Eqs. (29)–(34) and the field equations (20)–(24), these relations allow us to find all thermodynamic quantities as functions of baryon number density $n_{\rm b}$, as well as to determine the function $P(\rho)$.

APPENDIX C: ADIABATIC INDICES

Here we describe in more detail the calculation of the adiabatic indices $\gamma_{\rm eq}$, $\gamma_{\rm fr}$, and $\gamma_{\rm part\,fr}$. All the indices are given by Eq. (69), which can be represented as

$$\gamma = \frac{n_{\rm b}}{P}\,\frac{\delta P}{\delta n_{\rm b}}, \tag{C1}$$

where we make use of the fact that in thermodynamic equilibrium $P + \rho = \mu_{\rm n} n_{\rm b}$ and that for small deviations from thermodynamic equilibrium $\delta\rho = \mu_{\rm n}\delta n_{\rm b}$ (see, e.g., Gusakov 2007; Gusakov & Kantor 2008).

Model	g_3 (fm^{-1})	g_4	$g_{\sigma{\rm N}}$	$g_{\omega{\rm N}}$	$g_{\rho{\rm N}}$	$g_{\sigma\Lambda}$	$g_{\sigma\Sigma}$	$g_{\sigma\Xi}$	$g_{\sigma^*{\rm N}}$	$g_{\sigma^*\Lambda}$	$g_{\sigma^*\Sigma}$	$g_{\sigma^*\Xi}$
GM1A	9.840	-6.693	8.897	10.617	8.198	5.435	3.603	2.844	–	–	–	–
GM1′B	16.324	-31.985	9.096	10.558	8.198	6.241	4.368	4.275	–	–	–	–
TM1C	7.684	-2.224	10.038	12.300	9.275	7.733	6.037	6.320	0.0	1.585	1.585	6.999

Table A3. Coupling constants for the models **GM1A**, **GM1′B**, and **TM1C**.

(*i*) *Equilibrium adiabatic index* $\gamma_{\rm eq}$.
As it is discussed in Sec. 6.2 in that case the ratio $\delta P/\delta n_{\rm b}$ should be calculated in full thermodynamic equilibrium, that is, under conditions (B1) and (B2). In this situation, P can be presented as only a function of $n_{\rm b}$, while other particle number densities can be expressed through $n_{\rm b}$ by means of Eqs. (B1) and (B2). In other words, one can calculate $\gamma_{\rm eq}$ from the following formula,

$$\gamma_{\rm eq} = \frac{n_{\rm b}}{P}\,\frac{dP(n_{\rm b})}{dn_{\rm b}}. \tag{C2}$$

(*ii*) *Frozen adiabatic index* $\gamma_{\rm fr}$.
In this case all reactions of particle mutual transformations are frozen, that is, $y_i = n_i/n_{\rm b} =$ constant for any particle species i. The quasineutrality condition (B2) is then automatically satisfied and $\gamma_{\rm fr}$ can be calculated from the formula

$$\gamma_{\rm fr} = \frac{n_{\rm b}}{P}\,\frac{\partial P(n_{\rm b},\, y_{\rm e},\, y_\mu,\, y_{\rm n},\, y_{\rm p},\, y_\Lambda,\, \ldots)}{\partial n_{\rm b}}. \tag{C3}$$

(*iii*) *Partly frozen adiabatic index* $\gamma_{\rm part\,fr}$.
In this case all the slow reactions due to weak interaction (in particular, those with leptons e and μ) are frozen, which means that

$$y_{\rm e} = \text{constant}, \tag{C4}$$

$$y_\mu = \text{constant}. \tag{C5}$$

In contrast, the reactions due to strong interaction are so fast that the matter is always in equilibrium with respect to them. Here are these fast reactions

$$\mathrm{p} + \Xi^- \;\leftrightarrow\; \Lambda + \Lambda, \tag{C6}$$

$$\mathrm{n} + \Xi^0 \;\leftrightarrow\; \Lambda + \Lambda, \tag{C7}$$

$$\mathrm{p} + \Sigma^- \;\leftrightarrow\; \mathrm{n} + \Lambda, \tag{C8}$$

$$\mathrm{n} + \Sigma^0 \;\leftrightarrow\; \mathrm{n} + \Lambda, \tag{C9}$$

$$\mathrm{n} + \Sigma^+ \;\leftrightarrow\; \mathrm{p} + \Lambda, \tag{C10}$$

$$\Sigma^+ + \Sigma^- \;\leftrightarrow\; \Lambda + \Lambda. \tag{C11}$$

and the corresponding conditions of equilibrium

$$\mu_{\rm p} + \mu_{\Xi^-} = 2\mu_\Lambda, \tag{C12}$$

$$\mu_{\rm n} + \mu_{\Xi^0} = 2\mu_\Lambda, \tag{C13}$$

$$\mu_{\rm p} + \mu_{\Sigma^-} = \mu_{\rm n} + \mu_\Lambda, \tag{C14}$$

$$\mu_{\Sigma^0} = \mu_\Lambda, \tag{C15}$$

$$\mu_{\rm n} + \mu_{\Sigma^+} = \mu_{\rm p} + \mu_\Lambda, \tag{C16}$$

$$\mu_{\Sigma^+} + \mu_{\Sigma^-} = 2\mu_\Lambda. \tag{C17}$$

In stable NSs only Λ, Ξ^-, and (for the model **GM1′B**) Ξ^0-hyperons can be present, so only the first two conditions, (C12) and (C13), are relevant.

The final two conditions that should be taken into account are the conservation of electric charge (B2) and the strangeness fraction $y_{\rm S} = S/n_{\rm b}$,

$$y_{\rm S} = \text{constant}, \tag{C18}$$

where $S = \sum_i s_i n_i$ is the strangeness number density and s_i is the strangeness of particle species i. The condition (C18) follows from the observation that strangeness is conserved in reactions (C12)–(C17) (while other reactions are frozen).

The conditions (B2), (C4), (C5), and (C12)–(C18) allow one to express the pressure as a function of only four variables $n_{\rm b}$, $y_{\rm e}$, y_μ, and $y_{\rm S}$, and to present adiabatic index $\gamma_{\rm part\,fr}$ in the form

$$\gamma_{\rm part\,fr} = \frac{n_{\rm b}}{P}\,\frac{\partial P(n_{\rm b},\, y_{\rm e},\, y_\mu,\, y_{\rm S})}{\partial n_{\rm b}}. \tag{C19}$$

APPENDIX D: DESCRIPTION OF ON-LINE MATERIAL

The results of our numerical calculations are summarized in a number of files that can be found on the web: **http://www.ioffe.ru/astro/NSG/heos/hyp.html**. We briefly describe them here.

(1) Files **GM1A.dat**, **GM1′B.dat**, and **TM1C.dat** contain data concerning the pressure P, energy density ρ (both in MeV

Column number	1	2	3	4	5	6	7
Parameter	$n_{\rm b}$	P	ρ	$n_{\rm e}$	n_μ	$n_{\rm n}$	$n_{\rm p}$
Dimension	fm^{-3}	MeV fm^{-3}	MeV fm^{-3}	fm^{-3}	fm^{-3}	fm^{-3}	fm^{-3}
Column number	8	9	10	11	12	13	
Parameter	n_Λ	n_{Ξ^-}	n_{Σ^-}	n_{Ξ^0}	n_{Σ^0}	n_{Σ^+}	
Dimension	fm^{-3}	fm^{-3}	fm^{-3}	fm^{-3}	fm^{-3}	fm^{-3}	

Table D1. Structure of the files **GM1A.dat**, **GM1′B.dat**, and **TM1C.dat**.

Column number	1	2	3	4	5	6
Parameter	$n_{\rm b}$	σ	ω^0	ρ_3^0	σ^*	ϕ^0
Dimension	fm^{-3}	MeV	MeV	MeV	MeV	MeV

Table D2. Structure of the files **GM1A_Fields.dat**, **GM1′B_Fields.dat**, and **TM1C_Fields.dat**

fm^{-3}) and particle number densities n_i (in fm^{-3}) for *three* models **GM1A**, **GM1′B**, and **TM1C**, studied in this paper. Each file consists of 13 columns for 13 parameters listed in Tab. D1.

(2) Files **GM1A_Fields.dat**, **GM1′B_Fields.dat**, and **TM1C_Fields.dat** contain data concerning the values of meson fields (in MeV) at different baryon number densities $n_{\rm b}$ (see Table D2).

(3) Files **GM1A_gamma.dat**, **GM1′B_gamma.dat**, and **TM1C_gamma.dat** contain data concerning the values of adiabatic indices $\gamma_{\rm eq}$, $\gamma_{\rm part\,fr}$, and $\gamma_{\rm fr}$ at different baryon number densities $n_{\rm b}$ (see Table D3).

(4) Files **GM1A_Mass.dat**, **GM1′B_Mass.dat**, and **TM1C_Mass.dat** contain data concerning the values of Landau effective masses m_i^* [Eq. (30)] at different baryon number densities $n_{\rm b}$ (see Table D4).

(5) Files **GM1A_F0.dat**, **GM1′B_F0.dat**, and **TM1C_F0.dat** contain dimensionless Landau parameters F_0^{ij} (see Eq. 7). Note that $F_0^{ij} = F_0^{ji}$, so only $8\times 9/2 = 36$ matrix elements are independent and presented in these files (37 columns in each file; the first column is $n_{\rm b}$ in fm^{-3}). An actual column number containing the Landau parameters with indices i and j can be found from Tab. D5. For instance, Landau parameters $F_0^{\Sigma^-\,\Xi^0}$ are given in the column 29. Knowledge of the Landau parameters F_0^{ij} and effective masses m_i^* allows one to calculate the important thermodynamic derivatives, $\partial\mu_i(n_{\rm n},\ldots,n_{\Sigma^+})/\partial n_j$. As follows from Eqs. (7) and (68),

$$\frac{\partial\mu_i(n_{\rm n},\ldots,n_{\Sigma^+})}{\partial n_j} = \frac{\partial\mu_j(n_{\rm n},\ldots,n_{\Sigma^+})}{\partial n_i} = \frac{\pi^2\,\hbar^3}{\sqrt{m_i^* m_j^*\,p_{{\rm F}i}p_{{\rm F}j}}}\left(F_0^{ij}+\delta_{ij}\right). \tag{D1}$$

(6) Files **GM1A_F1.dat**, **GM1′B_F1.dat**, and **TM1C_F1.dat** contain dimensionless Landau parameters F_1^{ij} and have exactly the same structure as the files with F_0^{ij} (see Tab. D5).

(7) Files **GM1A_Entr.dat**, **GM1′B_Entr.dat**, and **TM1C_Entr.dat** contain the symmetric entrainment matrix Y_{ij} ($= Y_{ji}$). The first column is $n_{\rm b}$ in fm^{-3}; the next columns 2–37 are the elements of the entrainment matrix Y_{ij} [in cm^{-3} erg^{-1}; see Eq. (12)] ordered in the same way as in the case of Landau parameters F_0^{ij} and F_1^{ij} (see Tab. D5).

Column number	1	2	3	4
Parameter	$n_{\rm b}$	$\gamma_{\rm eq}$	$\gamma_{\rm part\,fr}$	$\gamma_{\rm fr}$
Dimension	fm^{-3}	dimensionless	dimensionless	dimensionless

Table D3. Structure of the files **GM1A_gamma.dat**, **GM1′B_gamma.dat**, and **TM1C_gamma.dat**

Column number	1	2	3	4	5	6	7	8	9
Parameter	$n_{\rm b}$	$m^*_{\rm n}$	$m^*_{\rm p}$	m^*_{Λ}	$m^*_{\Xi^-}$	$m^*_{\Sigma^-}$	$m^*_{\Xi^0}$	$m^*_{\Sigma^0}$	$m^*_{\Sigma^+}$
Dimension	fm^{-3}	g	g	g	g	g	g	g	g

Table D4. Structure of the files **GM1A_Mass.dat**, **GM1′B_Mass.dat**, and **TM1C_Mass.dat**

Column number	1	2	3	4	5	6	7	8	9	10	11	12	13
Parameter	$n_{\rm b}$	nn	np	nΛ	nΞ^-	nΣ^-	nΞ^0	nΣ^0	nΣ^+	pp	pΛ	pΞ^-	pΣ^-
Column number	14	15	16	17	18	19	20	21	22	23	24	25	26
Parameter	pΞ^0	pΣ^0	pΣ^+	$\Lambda\Lambda$	$\Lambda\Xi^-$	$\Lambda\Sigma^-$	$\Lambda\Xi^0$	$\Lambda\Sigma^0$	$\Lambda\Sigma^+$	$\Xi^-\Xi^-$	$\Xi^-\Sigma^-$	$\Xi^-\Xi^0$	$\Xi^-\Sigma^0$
Column number	27	28	29	30	31	32	33	34	35	36	37		
Parameter	$\Xi^-\Sigma^+$	$\Sigma^-\Sigma^-$	$\Sigma^-\Xi^0$	$\Sigma^-\Sigma^0$	$\Sigma^-\Sigma^+$	$\Xi^0\Xi^0$	$\Xi^0\Sigma^0$	$\Xi^0\Sigma^+$	$\Sigma^0\Sigma^0$	$\Sigma^0\Sigma^+$	$\Sigma^+\Sigma^+$		

Table D5. A schematic structure of the files **GM1A_F0.dat**, **GM1′B_F0.dat**, **TM1C_F0.dat**, **GM1A_F1.dat**, **GM1′B_F1.dat**, **TM1C_F1.dat**, **GM1A_Entr.dat**, **GM1′B_Entr.dat**, and **TM1C_Entr.dat**.